

PREPARED FOR SUBMISSION TO JHEP

# The fate of the Littlest Higgs Model with $T$ -parity under 13 TeV LHC Data

---

Daniel Dercks,<sup>a</sup> Gudrid Moortgat-Pick,<sup>a</sup> Jürgen Reuter,<sup>b</sup> and So Young Shim<sup>b</sup>

<sup>a</sup>*II. Institut für Theoretische Physik, Universität Hamburg, Luruper Chaussee 149, 22761 Hamburg, Germany*

<sup>b</sup>*DESY, Notkestraße 85, D-22607 Hamburg, Germany*

*E-mail:* [daniel.dercks@desy.de](mailto:daniel.dercks@desy.de), [gudrid.moortgat-pick@desy.de](mailto:gudrid.moortgat-pick@desy.de),  
[juergen.reuter@desy.de](mailto:juergen.reuter@desy.de), [soyoung.shim@desy.de](mailto:soyoung.shim@desy.de)

**ABSTRACT:** We exploit all LHC available Run 2 data at center-of-mass energies of 8 and 13 TeV for searches for physics beyond the Standard Model. We scrutinize the allowed parameter space of Little Higgs models with the concrete symmetry of  $T$ -parity by providing comprehensive analyses of all relevant production channels of heavy vectors, top partners, heavy quarks and heavy leptons and all phenomenologically relevant decay channels. Constraints on the model will be derived from the signatures of jets and missing energy or leptons and missing energy. Besides the symmetric case, we also study the case of  $T$ -parity violation. Furthermore, we give an extrapolation to the LHC high-luminosity phase at 14 TeV as well.

**KEYWORDS:** Little Higgs models, LHC searches, New Physics Signatures

**ARXIV EPRINT:** [1801.XXXXX](https://arxiv.org/abs/1801.XXXXX)

---

## Contents

<b>1</b>	<b>Introduction</b>	<b>1</b>
<b>2</b>	<b>Little Higgs Models with <math>T</math>-Parity</b>	<b>3</b>
2.1	$T$ -parity Violation	6
2.2	Naturalness and Fine Tuning	7
<b>3</b>	<b>Electroweak Precision Constraints</b>	<b>8</b>
<b>4</b>	<b>Tool Framework and Scan Setup</b>	<b>9</b>
4.1	Used Software	9
4.2	Details on Event Generation	10
4.3	Scan Benchmark Scenarios	12
<b>5</b>	<b>Collider Topologies</b>	<b>14</b>
5.1	Cross Sections	14
5.2	Branching Ratios	16
5.3	Expected Final State Topologies and Correspondence to Supersymmetric Searches	20
<b>6</b>	<b>Collider Results from CheckMATE</b>	<b>22</b>
6.1	Fermion Universality	23
6.2	Heavy $q_H$	27
6.3	Light $\ell_H$	31
6.4	Prospects for $\sqrt{s} = 14$ TeV	32
<b>7</b>	<b>Comparison of LHC limits with Bounds from Electroweak Precision Observables</b>	<b>35</b>
<b>8</b>	<b>Summary</b>	<b>38</b>
<b>A</b>	<b>Supplementary Figures for the Collider Analysis</b>	<b>40</b>
<b>B</b>	<b>Full List of CheckMATE Analyses</b>	<b>40</b>

---

## 1 Introduction

The main legacy of the 7/8 and 13 TeV runs of the Large Hadron Collider (LHC) is the discovery of a 125 GeV Higgs boson [1, 2] as well as the absence of any signals for other new particles. This is in accordance with the measurements of electroweak precision observables

(EWPO) which agree very well with a Standard Model (SM) containing a light Higgs boson and no further degrees of freedom in the range up to a TeV. Besides the EWPO from the pre-LHC era and flavor physics observables, both direct searches and the ever more precise measurements of the properties of the Higgs boson (as well as the top quark and weak gauge bosons) are the tools to search for physics beyond the Standard Model (BSM) at the LHC. These are used to constrain any type of BSM model.

In this paper we study the Littlest Higgs Model with  $T$ -parity (LHT). This is an attractive representative of Little Higgs models [3, 4] since fine tuning problems in the Higgs potential can be avoided via a discrete global  $Z_2$  symmetry. Little Higgs models in general regard a naturally light Higgs boson as a pseudo-Nambu-Goldstone boson (pNGB) arising from a (new) global symmetry at high scale, see e.g. Ref. [5, 6]. However, such a mechanism would require new strong interactions to tie the constituents of the Higgs boson together, which unavoidably would show up in electroweak precision observables. In order to avoid such strong constraints from EWPO, the mechanism of so-called collective symmetry breaking has been applied, i.e. interweaving several global symmetries which all have to be broken in order to give mass to the pNGBs charged under them. This means that the Higgs mass achieves only a logarithmic sensitivity to the cutoff scale at one-loop, while a quadratic sensitivity only arises at the two-loop level, thereby shifting the strongly-interacting UV completion scale from the multi-TeV to the multi-10 TeV-region. Note, however, that Little Higgs models are effective field theories (with new degrees of freedom beyond the SM like heavy vectors, scalars and quarks) that not necessarily have a direct strongly coupled UV completion, but could also have weakly-coupled sectors at the next scale [7].

In this paper we consider the LHT model just as such an effective (low-energy) field theory consisting of the SM degrees of freedom augmented by ( $T$ -odd) heavy vector bosons, heavy quarks (and leptons) as well as additional heavy pNGBs (which turn out to be irrelevant for the phenomenology of that model). All of these particles just have the SM gauge interactions as well as generalizations of the SM Yukawa couplings, which reflect the implementation of both the Little Higgs collective symmetries as well as  $T$ -parity. We consider all phenomenologically relevant production mechanisms for the heavy new particles, including all relevant decays in order to compare the predictions within the LHT model with the LHC 13 TeV data from Run 2. In addition, we reproduce the constraints from the EWPO. For completeness, we review the status from the 8 TeV Run 1 data. Because of the possibility of  $T$ -parity breaking in a strongly coupled UV completion of the LHT, as well as tensions from dark matter (DM) constraints, we also take signatures and limits from a scenario with  $T$ -parity breaking into account which is different than the Littlest Higgs model without  $T$ -parity. We also give prospects for the upcoming high-luminosity runs at the LHC at 14 TeV.

The outline of the paper is as follows: in order to make the paper self-contained, in Sec. 2 we briefly summarize the model-building setup of the Littlest Higgs model (with  $T$ -parity) needed to understand the phenomenological analyses later on. In Sec. 3 we review the existing limits from EWPO on the LHT model. In the next section, Sec. 4, we discuss the tool chain for generating events and recasting the LHC analyses. We then collect

the relevant collider topologies along with cross sections and branching ratios for different regions of parameter space in Sec. 5. Our main collider results are collected in Sec. 6, and compared to the sensitivity from electroweak precision data in Sec. 7. Finally, we give a summary and outlook in Sec. 8.

## 2 Little Higgs Models with $T$ -Parity

The Littlest Higgs model [8] is based on a non-linear sigma model with a single field  $\Sigma$  parameterizing a  $SU(5)/SO(5)$  symmetry breaking structure.<sup>1</sup> The vacuum expectation value (vev) causing the breaking from  $SU(5)$  to  $SO(5)$ ,  $\Sigma_0$ , can be cast into the form of the  $5 \times 5$  matrix

$$\Sigma_0 = \begin{pmatrix} & & \mathbf{1}_{2 \times 2} \\ & 1 & \\ \mathbf{1}_{2 \times 2} & & \end{pmatrix}. \quad (2.1)$$

The gauge group of the Littlest Higgs is  $G_1 \times G_2 = (SU(2)_1 \times U(1)_1) \times (SU(2)_2 \times U(1)_2)$  embedded in  $SU(5)$  as a subgroup such that the vev in Eq. (2.1) above breaks it down into the diagonal subgroup  $SU(2)_L \times U(1)_Y$  which is identified with the SM electroweak group. The kinetic term for the non-linear sigma model field is

$$\mathcal{L}_{kin} = \frac{f^2}{4} \text{Tr} |D_\mu \Sigma|^2 \quad (2.2)$$

with

$$\Sigma = e^{i\Pi/f} \Sigma_0 e^{i\Pi^T/f} = e^{2i\Pi/f} \Sigma_0 \quad (2.3)$$

where  $f$  is the Nambu-Goldstone-Boson (NGB) decay constant of the model. At this scale the symmetry breakings  $SU(5) \rightarrow SO(5)$  and  $G_1 \times G_2 \rightarrow SU(2)_L \times U(1)_Y$  take place. The covariant derivative in Eq. (2.2) is given by

$$D_\mu \Sigma = \partial_\mu \Sigma - i \sum_j [g_j W_j^a (Q_j^a \Sigma + \Sigma Q_j^{aT}) + g'_j B_j (Y_j \Sigma + \Sigma Y_j)] \quad (2.4)$$

with the generators

$$Q_1^a = \frac{1}{2} \begin{pmatrix} \sigma^a & \mathbf{0}_{2 \times 3} \\ \mathbf{0}_{3 \times 2} & \mathbf{0}_{3 \times 3} \end{pmatrix}, \quad Q_2^a = \frac{1}{2} \begin{pmatrix} \mathbf{0}_{3 \times 3} & \mathbf{0}_{2 \times 3} \\ \mathbf{0}_{3 \times 2} & -(\sigma^a)^* \end{pmatrix} \quad (2.5)$$

$$Y_1 = \frac{1}{10} \text{diag}(-3, -3, 2, 2, 2), \quad Y_2 = \frac{1}{10} \text{diag}(-2, -2, -2, 3, 3) \quad , \quad (2.6)$$

where  $\sigma^a$  are Pauli matrices. The  $SU(5) \rightarrow SO(5)$  symmetry breaking generates a total of 14 NGBs  $\Pi^a$  which decompose under the unbroken EW group  $SU(2)_L \times U(1)_Y$  as  $\mathbf{1}_0 \oplus \mathbf{3}_0 \oplus \mathbf{2}_{\pm\frac{1}{2}} \oplus \mathbf{3}_{\pm 1}$ . Four of these NGBs are eaten by the extra gauge bosons,  $Z_H$ ,  $W_H$  and  $A_H$ , which get masses of the order  $f$ . The remaining ten physical (p)NGBs decompose

<sup>1</sup>For different implementations of Little Higgs models in terms of product group and simple group models and a way to distinguish them, cf. e.g. [9–11].

into the complex Higgs doublet and a hypercharge one complex triplet. The latter is phenomenologically irrelevant as the production cross section for these particles is negligibly small, cf. Ref. [19].

Like many other BSM models, the Littlest Higgs model suffers from constraints by electroweak precision observables, particularly as the heavy hypercharge boson,  $A_H$ , has an accidentally small prefactor, cf. the right hand side of Eq. (2.10). To alleviate these constraints, a discrete symmetry, TeV- or short  $T$ -parity has been added [12, 13], which phenomenologically plays a similar role as  $R$ -parity in supersymmetry (SUSY).  $T$ -parity is an involutory automorphism that exchanges the sets of the two different gauge algebras  $G_1$  and  $G_2$ , or alternatively, their gauge bosons:

$$W_{1\mu}^a \xleftrightarrow{T} W_{2\mu}^a, \quad B_{1\mu} \xleftrightarrow{T} B_{2\mu}. \quad (2.7)$$

This fixes the gauge coupling constants of the two different  $SU_{1,2}(2)$  and  $U_{1,2}(1)$  to be equal:

$$g_1 = g_2 = \sqrt{2}g, \quad (2.8)$$

$$g'_1 = g'_2 = \sqrt{2}g'. \quad (2.9)$$

The mass eigenstates are then just the (normalized) sum and difference of the two gauge fields, respectively, with mixing angles of  $\pi/4$ . This results in the mass terms of the heavy gauge bosons

$$m_{W_H} = m_{Z_H} = gf, \quad (2.10a)$$

$$m_{A_H} = \frac{g'f}{\sqrt{5}}. \quad (2.10b)$$

In order to implement collective symmetry breaking in the fermion fields, a partner state to the third generation quark doublet has to be introduced, forming an incomplete  $SU(5)$  multiplet  $\Psi$  and its  $T$ -parity partner  $\Psi'$

$$\Psi = \begin{pmatrix} ib_L \\ -it_{1L} \\ t_{2L} \\ \mathbf{0}_{2 \times 1} \end{pmatrix} = \begin{pmatrix} q_L \\ t_{2L} \\ \mathbf{0}_{2 \times 1} \end{pmatrix}, \quad \Psi' = \begin{pmatrix} \mathbf{0}_{2 \times 1} \\ t'_{2L} \\ ib'_L \\ -it'_{1L} \end{pmatrix} = \begin{pmatrix} \mathbf{0}_{2 \times 1} \\ t'_{2L} \\ q'_L \end{pmatrix}, \quad (2.11)$$

which are related via

$$\Psi \xleftrightarrow{T} -\Sigma_0 \Psi' \quad (2.12)$$

Here,  $q_L$  denotes the quark doublet of the SM following the conventions in [8], while  $q'_L$  and  $t'_{2L}$  are the  $T$ -parity partner fermions needed to reconcile both  $T$ -parity and the collective symmetry breaking mechanism. The  $T$ -parity invariant Lagrangian then reads as

$$\mathcal{L}_Y \supset \frac{\lambda_1 f}{2\sqrt{2}} \epsilon_{ijk} \epsilon_{xy} (\bar{\Psi}_i \Sigma_{jx} \Sigma_{ky} - (\bar{\Psi}')_i \tilde{\Sigma}_{jx} \tilde{\Sigma}_{ky}) t_{1R} + \lambda_2 f (\bar{t}_{2L} t_{2R} + \bar{t}'_{2L} t'_{2R}) + h.c., \quad (2.13)$$

where  $\lambda_{1,2}$  denote the top-quark Yukawa couplings, respectively. The  $T$ -parity eigenstates are now the (normalized) differences (even states) and sums (odd states) of the primed

and unprimed fermion fields  $t_+ = (t_{1L,+}, t_R)$ ,  $t_- = (t_{1L,-}, t_{1R,-})$ ,  $T^- = (t_{2L,-}, t_{2R,-})$  and  $T'_+ = (t_{2L,+}, t_{2R,+})$ . Diagonalizing the left-handed  $T$ -even fermions yields the (SM) top quark and the heavy  $T$ -even top quark,  $T^+$ . The  $t_-$  gets a mass with the help of the so-called mirror fermions, cf. below for the first and second generation fermions, while the masses for the SM top quark and the other top partners are given by,

$$m_{t_{SM}} = m_{t_+} = \frac{\lambda_2 R}{\sqrt{1+R^2}} v, \quad (2.14)$$

$$m_{T^-} = \lambda_2 f = \frac{m_{t_+}}{v} \frac{f \sqrt{1+R^2}}{R} \quad (2.15)$$

$$m_{T^+} = \frac{m_{t_+}}{v} \frac{f(1+R^2)}{R} = m_{T^-} \sqrt{1+R^2} \quad . \quad (2.16)$$

$R$  is defined as the ratio between the Yukawa coefficients of the two different possible terms,  $R = \lambda_1/\lambda_2$  and is one of the parameters used for investigating the parameter space in this paper.

Up-type quarks for the first and second generations have a similar Lagrangian than the top quark except for the vector-like quark, which is not present as there is no need to cancel the contribution from light quarks to Higgs self energies:

$$\mathcal{L}_Y \supset \frac{i\lambda_d f}{2\sqrt{2}} \epsilon_{ij} \epsilon_{xyz} (\bar{\Psi}'_x \Sigma_{jy} \Sigma_{jz} X - (\bar{\Psi} \Sigma_0)_x \tilde{\Sigma}_{iy} \tilde{\Sigma}_{jz} \tilde{X}) d_R \quad (2.17)$$

The  $SU(2)_{1,2}$  singlet  $X$  with  $U(1)_{1,2}$  charges  $(Y_1, Y_2) = (1/10, -1/10)$  renders the term gauge invariant. There are two different  $X$  embeddings as  $(3, 3)$  component into the NGB multiplet, namely  $X = (\Sigma_{33})^{-1/4}$  [Case A] and  $X = (\Sigma_{33})^{1/4}$  [Case B]. These cases do not differ in the context of BSM collider phenomenology which is why we choose Case A in this study. Differences only arise in the discussion of constraints from the Higgs sector and electroweak precision observables and more details can be found in Ref. [19].

To give rise to mass terms for the  $T$ -odd fermions without introducing any anomalies, another  $SO(5)$  multiplet  $\Psi_c$  is introduced as

$$\Psi_c = \left( id_c, -iu_c, \chi_c, i\tilde{d}_c, -i\tilde{u}_c \right)^T = (q_c, \chi_c, \tilde{q}_c)^T, \quad \Psi_c \xleftrightarrow{T} -\Psi_c. \quad (2.18)$$

The  $q_c$  fields are called mirror fermion.

The  $T$ -parity invariant Lagrangian for the light fermions is

$$\mathcal{L}_\kappa = -\kappa f (\bar{\Psi}' \xi \Psi_c + \bar{\Psi} \Sigma_0 \Omega \xi^\dagger \Omega \Psi_c) + h.c.. \quad (2.19)$$

This Lagrangian not only adds the  $T$ -odd mass terms but also imposes new interactions between Higgs boson and up-type partners.

$$\mathcal{L}_\kappa \supset -\sqrt{2}\kappa f (\bar{d}_{L-} \tilde{d}_c + \frac{1+c_\xi}{2} \bar{u}_{L-} \tilde{u}_c - \frac{s_\xi}{\sqrt{2}} \bar{u}_{L-} \chi_c - \frac{1-c_\xi}{2} \bar{u}_{L-} u_c) + h.c. + \dots \quad (2.20)$$

where  $c_\xi = \cos((v+h)/\sqrt{2}f)$ ,  $s_\xi = \sin((v+h)/\sqrt{2}f)$ .

The parameter  $\kappa$  characterizing the coupling between the Higgs and the  $T$ -odd fermions is another degree of freedom in the model parameter space we investigated. We will distinguish between  $\kappa_q$  for the light quarks and  $\kappa_l$  for the leptons.

The mass spectrum for heavy  $T$ -odd fermions is given (at order  $\mathcal{O}(v^2/f^2)$ ) by

$$m_{u,-} = \sqrt{2} \kappa_q f \left(1 - \frac{1}{8} \frac{v^2}{f^2}\right), \quad (2.21)$$

$$m_{d,-} = \sqrt{2} \kappa_q f \quad (2.22)$$

$$m_{\ell,-} = \sqrt{2} \kappa_l f \quad (2.23)$$

## 2.1 $T$ -parity Violation

For the phenomenology of the LHT model, we will also consider  $T$ -parity violation. There are two reasons for that: first, in the context of strongly interacting UV completions  $T$ -parity violation can naturally occur via an anomalous Wess-Zumino-Witten term, [14, 15], secondly, there is a certain tension for the case that the lightest  $T$ -odd particle, the heavy photon  $A_H$  is absolutely stable from relic density calculations and direct detection dark matter experiments [16, 17]. In order to avoid any constraints from dark matter bounds, one can assume that the  $A_H$  only has a microscopic lifetime and that dark matter instead is made up of an axion-like particle in the strongly interacting UV completion of the Little Higgs model.

As has been studied in [14, 18],  $T$ -parity violation generates decays the heavy photon partner  $A_H$  into the electroweak gauge bosons  $WW$  and  $ZZ$  similar to the decay of the pion into two photons. Above the kinematic threshold for these  $A_H$  decays, the partial width is given by:

$$\Gamma(A_H \rightarrow ZZ) = \left(\frac{Ng'}{80\sqrt{3}\pi^3}\right)^2 \frac{M_{A_H}^3 m_Z^2}{f^4} \left(1 - \frac{4m_Z^2}{M_{A_H}^2}\right)^{\frac{5}{2}}, \quad (2.24)$$

$$\Gamma(A_H \rightarrow W^+W^-) = \left(\frac{Ng'}{40\sqrt{3}\pi^3}\right)^2 \frac{M_{A_H}^3 m_W^2}{f^4} \left(1 - \frac{4m_W^2}{M_{A_H}^2}\right)^{\frac{5}{2}}. \quad (2.25)$$

Here, the integer  $N$  depends on the UV completion of the theory. As we are only interested in branching ratios, shown in a later section, the precise choice of this number does not matter for our analysis.

If the mass of  $A_H$  is below the  $WW$  and  $ZZ$  thresholds, it will decay into the SM fermions via  $WW$ - and  $ZZ$ -induced triangle loops leading to the partial widths:

$$\Gamma(A_H \rightarrow ff) = \left(\frac{N_{C,f} M_{A_H}}{48\pi}\right) \left[ c_-^2 \left(1 - \frac{4m_f^2}{M_{A_H}^2}\right) + c_+^2 \left(1 + \frac{2m_f^2}{M_{A_H}^2}\right) \right] \left(1 - \frac{4m_f^2}{M_{A_H}^2}\right)^{\frac{1}{2}}, \quad (2.26)$$

with  $c_{\pm} := c_R \pm c_L$ , and  $c_L$  and  $c_R$  being the left- and right-handed fermion couplings, shown in Table 1.  $N_{C,f}$  is the number of colors of the final state fermions. For the range  $f \sim 1 - 10$  TeV and  $N = \mathcal{O}(1)$ , the total  $A_H$  width  $\Gamma_{A_H}$  ranges between 0.01-1 eV which

Particles	$c_L^f$	$c_R^f$
$A_H e^+ e^-$	$\frac{9\hat{N}}{160\pi^2} \frac{v^2}{f^2} g^4 g' (4 + (c_w^{-2} - 2t_w^2)^2)$	$-\frac{9\hat{N}}{40\pi^2} \frac{v^2}{f^2} g'^5$
$A_H \bar{\nu} \nu$	$\frac{9\hat{N}}{160\pi^2} \frac{v^2}{f^2} g^4 g' (4 + c_w^{-4})$	0
$A_H \bar{u}_a u_b$	$-\frac{\hat{N}}{160\pi^2} \frac{v^2}{f^2} g^4 g' (36 + (3c_w^{-2} - 4t_w^2)^2) \delta_{ab}$	$-\frac{\hat{N}}{10\pi^2} \frac{v^2}{f^2} g'^5 \delta_{ab}$
$A_H \bar{d}_a d_b$	$-\frac{\hat{N}}{160\pi^2} \frac{v^2}{f^2} g^4 g' (36 + (3c_w^{-2} - 2t_w^2)^2) \delta_{ab}$	$-\frac{\hat{N}}{40\pi^2} \frac{v^2}{f^2} g'^5 \delta_{ab}$

**Table 1.** Coefficients for the  $A_H$  TPV decays, cf. Eq. (2.26). The indices  $a, b$  refer to the color of the respective quarks and we use  $\hat{N} = N/48\pi^2$ ,  $c_W = \cos \theta_W$ ,  $t_W = \tan \theta_W$ .

corresponds to a lifetime of order  $10^{-17}$  s. This excludes  $A_H$  from being a viable dark matter candidate. On the other hand, it leads to a mean free path of approximately 10 nm, resulting in nearly prompt decays which do not produce observable displaced vertices in the LHC detectors.

## 2.2 Naturalness and Fine Tuning

Together with the model setup, we discuss in this section the definition of fine tuning, that is sometimes used as a guideline for the naturalness of a model or of certain regions of parameter space. The naturalness is generally tied to the radiative corrections to the scalar potential in quantum field theories. In order for a model to be considered natural, those corrections should be of the same order as the scalar mass term from the mechanism that originally created that mass term (the explicit breaking of the global symmetries in Little Higgs models). A fine-tuning measure usually compares the size of the radiative corrections to this bare mass term. In the absence of a special cancellation mechanism, this measure depends quadratically on the typical scale of these corrections; cancellation by means of a symmetry turns this into a logarithmic dependence, or even zero if the symmetry is mighty enough like exact supersymmetry or conformal symmetries.

In Little Higgs models, the cancellation comes from SM partner particles of like statistics by means of nonlinearly realized global symmetries. The most severe SM radiative corrections from the top quark are cancelled by the  $T$ -odd and even top partners,  $T^\pm$ , followed by the cancellations of the EW gauge bosons due to the heavy new gauge bosons,  $A_H$ ,  $Z_H$ , and  $W_H$ . In this paper, we adopt the fine-tuning measure defined in [8], which only accounts for the top partners, and neglects the contributions from the gauge boson partners as well as from the heavy pNGBs and the light fermion partners. The fine tuning is then defined as the ratio of the experimentally measured Higgs mass squared and the absolute value of the radiative corrections from the top partners to the Higgs quadratic operator:

$$\Delta = \frac{\mu_{exp}^2}{|\delta\mu^2|}, \quad \delta\mu^2 = -\frac{3\lambda_t M_T^2}{8\pi^2} \log \frac{\Lambda^2}{M_T^2}. \quad (2.27)$$

Here  $\Lambda = 4\pi f$  is the cut-off scale of the LHT model, i.e. the equivalent to  $\Lambda_{\text{QCD}}$  in a strongly-interacting embedding of the LHT,  $\lambda_t$  is the SM top Yukawa coupling and  $M_T$



is a generic mass scale of the top partner sector. Note that this definition of the fine-tuning measure leads to the fact that smaller values of that measure (provided in per cent in general) constitute a higher amount of fine tuning, hence a more finely tuned point of parameter space. While the LHC Run 1 datasets at 7 and 8 TeV together with electroweak precision observables still allowed parameter space with  $\mathcal{O}(1\%)$  [19], we will see in this paper that the fine tuning including LHC Run 2 data is now everywhere around one per cent or even in the sub-per cent regime. This is still comparable with or better than the amount of fine tuning in generic parameter regions of the minimal supersymmetric SM (MSSM), and it is generically (much) better than the fine tuning for Composite Higgs models.

### 3 Electroweak Precision Constraints

Even before the start of data taking at the LHC, Little Higgs models were already grossly constrained by comparing their predictions to precise measurements in the electroweak sector, the so-called electroweak precision observables (EWPO) [20–23]. Additional constraints come from flavor data (in the  $K$ ,  $D$  and  $B$  sector), as well as for the models with  $T$  parity and stable massive particles from dark matter searches. We will not discuss the first point here as this has been studied elsewhere [24, 25], and the second point has been addressed in the last section.

EWPO mainly contain a list of measurements from  $e^+e^-$  colliders like LEP1, LEP2, SLC, and TRISTAN, and a few selected measurements from hadron colliders where the precision has superseded that from lepton colliders, like the  $W$  mass, or was only possible there, like the Higgs mass and couplings. In Refs. [19, 26, 27], both the EWPO as well as the latest Higgs data have been scrutinized in order to give the then best constraints on the parameter space of the LHT model.

We will not repeat the complete table of the EWPO fit of the LHT model from [19] here, but just remind that the two main observables with the highest pull in the fit giving the highest constraint are the total hadronic cross section at the  $Z$  pole as well as the left-right asymmetry on the  $b$  quarks,  $A_{LR}^{(b)}$ . Higgs observables in general do not give any further constraints beyond that as EWPO already drive the Little Higgs scale  $f$  in a region where the deviations of the Higgs couplings are well within the LHC experimental uncertainties. The only exception to this statement comes from the case when the decay  $H \rightarrow A_H A_H$  is possible which is ruled out by the LHC limits on Higgs invisible branching ratios and excludes  $m_{A_H} < 62.5 \text{ GeV}$ , i.e.  $f < 480 \text{ GeV}$  [19].

The first EWPO constraints that have been applied to Little Higgs models came from oblique corrections, the so-called Peskin-Takeuchi  $\Delta S$ ,  $\Delta T$  and  $\Delta U$  parameters [28, 29]. These parameterize corrections to the self energies of EW gauge bosons, that are measured in two-(and four-) fermion processes at lepton colliders.  $T$ -parity was specifically introduced to minimize the contributions from Little Higgs heavy particles to the oblique parameters as far as possible, as no  $T$ -odd particle can contribute to them at tree level. However, at loop-level there are contributions from  $T$ -odd heavy quarks, the  $T$ -even top quark, the mirror fermions and the heavy gauge bosons. These have been calculated in [30, 31].

One interesting feature derived in [19, 26] from the contribution of the heavy top partners to the  $\Delta T$  parameter, is the exclusion limit from EWPO as a function of the parameter  $R$ , the ratio of the two different Yukawa couplings  $\lambda_1$  and  $\lambda_2$  in the top sector. There is an accidental cancellation to the EWPO in terms of  $R$  for the value of  $R=1$ . This gives an only relatively weak exclusion limit for  $f \gtrsim 405$  GeV at 95% confidence level from EWPO only. For  $R \ll 1$  this bound goes up to roughly 750 GeV while for large  $R \sim 3$  the bound from EWPO goes up to 1.3 TeV.

For our discussion in this paper and the motivation into which regions of parameter space to look at, even more relevant are the contributions from the mirror fermions:

$$\Delta T_{q_H, \ell_H} = - \sum_{q_H, \ell_H} \frac{\kappa_{q, \ell}^2}{192\pi^2 \alpha_w} \frac{v^2}{f^2} \quad . \quad (3.1)$$

These expressions come from box diagrams contributing to four-fermion operators with heavy quark and lepton mirror fermions running in the loop:

$$\mathcal{O}_{4\text{-ferm.}} = - \frac{\kappa_{q, \ell}^2}{128\pi^2 f^2} \left( \bar{\psi}_L \gamma^\mu \psi_L \right) \left( \bar{\psi}'_L \gamma_\mu \psi'_L \right) \quad (3.2)$$

Here,  $\psi$  and  $\psi'$  are any combinations of different SM fermions. These four-fermion operators can be reinterpreted in terms of a contribution to the oblique  $\Delta T$  parameter. The peculiar feature about them is that they increase with the mass of the mirror fermions for fixed scale  $f$ . This is clear from the fact that in that case the Yukawa-type coupling which enters the box diagrams has to be enlarged leading to a larger contribution from the box diagrams. The  $\kappa$  is usually assumed to be a diagonal matrix in flavor space or even proportional to the unit matrix. In this paper, we do not lift the degeneracy in generation space, however, we investigate different values for the  $\kappa$  couplings for mirror quarks and mirror leptons.

As was shown in [19, 26, 27], the end of LHC Run 1 was sort of a turning point where limits from direct searches of heavy particles in Little Higgs models started to become competitive with EWPO, and now with Run 2 even superseded them. As the only relevant EWPO result is Eq. (3.2) and the  $R$  dependence from the top partner contributions to the  $\Delta T$  parameter, we do not discuss EWPO any further here, and take Eq. (3.2) as a motivation to look into different scenarios of combinations of all-light degenerate mirror fermions, heavy mirror quarks, as well as light mirror leptons and decoupled quarks and vice versa.

## 4 Tool Framework and Scan Setup

The main goal of this paper is to derive limits on the LHT model from all available LHC run II data. In this section we describe the framework that we used in order to derive numerically the current LHC bounds on the LHT model.

### 4.1 Used Software

To be able to generate Monte-Carlo events for our model, we make use of the FeynRules implementation of the LHT model as in Ref. [19, 26, 27]. We slightly extended the model

definition such that the heavy fermion Yukawa couplings  $\kappa$  are transformed into independent coupling constants  $\kappa_\ell$  and  $\kappa_q$ . We then exported the LHT model to the event generators `MG5_aMC@NLO` [32] and `WHIZARD` [33–36]<sup>2</sup> via the UFO file format.<sup>3</sup>

The collider phenomenology of the LHT model studied in this paper depends on the mass scale  $f$ , the two Yukawa coupling parameters  $\kappa_\ell$  and  $\kappa_q$ , as well as the ratio of top Yukawa couplings  $R$ . For these four parameters we derive the corresponding masses according to Eqs. (2.10), (2.16), (2.22) and store these in a spectrum file which follows the definitions of the UFO model. The branching ratios and corresponding decay tables for all LHT particles are calculated analytically using the formulae in the above linked model file. These include all 2-body decays for all relevant particles. Note that within the parameter space that we analyze, no 3-body decays need to be considered as there is always a dominating 2-body final state. The only difference is the anomaly-mediated decay of  $A_H$  in the case of  $T$ -parity violation, see Sec. 2.1. For this, we use the branching ratios as functions of  $f$  taken from Ref. [18] which will be shown later in this work. For decays into gauge bosons, we assume that for  $m(A_H) > 185$  GeV, i.e. for  $f \gtrsim 1080$  GeV,  $A_H$  decays via 2-body decays into  $WW$  and  $ZZ$ . For smaller masses, we formulate 3-body decays for the decay table as follows: we consider all possible decay modes of the  $W$  or  $Z$ , replace one of the final state gauge bosons with the corresponding decay products and multiply the branching ratio accordingly.

For the main tasks of this numerical study, we make use of the collider analysis tool `CheckMATE` [43–45]. This program is useful to test a given BSM model in an automatized way. It makes again use of the aforementioned generator `MG5_aMC@NLO` to simulate partonic events. By making use of the UFO model description file format, `MG5_aMC@NLO` or `WHIZARD` are able to simulate partonic events for a given BSM model which was implemented in a model building framework like `FeynRules` [46, 47] or `SARAH` [48], e.g. via the `WHIZARD-FeynRules` interface [49]. The showering and hadronization of these events is subsequently performed by `Pythia8` [50], followed by the fast detector simulation `Delphes` [51] which considers the effect of measurement uncertainties, finite reconstruction efficiencies and the jet clustering of the observed final state objects. These detector events are then quantified by various analyses from both `ATLAS` and `CMS` at center-of-mass energies of 8 and 13 TeV (more details below). Events are categorized in different signal regions and `CheckMATE` determines which signal region provides the strongest expected limit. If the input model predicts more signal events than are allowed by the observed limit of that signal region, `CheckMATE` concludes that the model is *excluded* at the 95% confidence level, otherwise the model is *allowed*. For more details on the inner functionality of `CheckMATE`, we refer to the manual papers in Refs. [43–45].

## 4.2 Details on Event Generation

For the event generation, we consider the production of all relevant two-body final states. In the following, we use  $q_H$  for all heavy fermion squarks  $\{d_H, u_H, s_H, c_H, b_H, t_H\}$ ,  $\ell_H$  for all other heavy fermions  $\{e_H, \mu_H, \tau_H, \nu_{eH}, \nu_{\mu H}, \nu_{\tau H}\}$ ,  $V_H$  for all heavy gauge bosons

<sup>2</sup>`WHIZARD` recently also has been extended towards next-to-leading order functionality, cf. [37–42].

<sup>3</sup>The model file is available on demand from the authors.

$\{W_H, Z_H$  and  $A_H\}$  and  $T^\pm$  for the additional heavy  $T$ -even/odd top partner, respectively. We analyzed the following processes for the LHC (cf. also [19, 26])

$$\begin{aligned}
1. \quad & pp \rightarrow q_H q_H, q_H \bar{q}_H, \bar{q}_H \bar{q}_H \\
2. \quad & pp \rightarrow q_H V_H \\
3. \quad & pp \rightarrow \ell_H \bar{\ell}_H \\
4. \quad & pp \rightarrow V_H V_H \\
5. \quad & pp \rightarrow T^+ \bar{T}^+, T^- \bar{T}^- \\
6. \quad & pp \rightarrow T_+ \bar{q}, \bar{T}_+ q, T_+ W^\pm, \bar{T}_+ W^\pm
\end{aligned} \tag{4.1}$$

At this stage we give some remarks on the choice of these final states.

- If  $T$ -parity is conserved,  $T$ -odd particles need to be produced in pairs. Therefore, the  $T$ -even top partner  $T^+$  is the only LHT particle which can be produced in association with Standard Model particles. This rule also holds in case of anomaly-triggered  $T$ -parity violation as the corresponding TPV couplings  $A_H - V - V$  are too small to result in another  $T$ -odd final state with experimentally accessible cross section.
- We focus our discussion on certain benchmark scenarios and within these scenarios, some processes are expected to be negligible compared to others. We give more details on this when we discuss the individual scan setups below.
- While the production of color-charged objects is expected to be dominant at the LHC in case  $q_H$  and  $V_H$  have similar masses, heavy gauge boson production can become dominant in regions of parameter space where the heavy gauge bosons are significantly lighter than the heavy quarks (i.e. for large  $\kappa$ ). We discuss the parameter dependence of the respective cross sections below.
- Processes with additional hard radiation in the final state, e.g. the process  $pp \rightarrow q_H q_H j$ , are not considered here. They are expected to be relevant in regions with strong mass degeneracy between the produced particle and the stable particle it decays into as in such a case the process  $pp \rightarrow q_H q_H$  produces too soft jets to be observed. By requiring an additional hard jet in the event,  $pp \rightarrow q_H q_H j$ , the additional jet can boost the  $q_H q_H$  system and create a new, potentially observable multijet topology (see e.g. Ref. [52]). However, in our case the gauge bosons  $W_H$  and  $Z_H$  are always predicted to be at least 100 GeV heavier than the  $A_H$ , cf. Eqs. (2.10a), (2.10b). Similarly, the  $q_H - A_H$  and  $T^- - A_H$  mass splittings are always large enough in the studied parameter regions. Therefore, we do not need to look at these peculiar topologies which have a significantly smaller cross section than our discussed two-body final states.
- Another interesting final state is  $pp \rightarrow A_H A_H j$  whose analysis is motivated because of the distinct and typical monojet signature as generally expected in models with a

dark matter candidate (see e.g. Ref. [53]). However, since our dark matter candidate has a mass of the order of about 100 GeV and since it couples directly to quarks via the  $A_H - q - q_H$  vertex, we do not expect LHC searches for dark matter final states to be more constraining than existing bounds from direct detection searches. Furthermore, the consideration of this final state is technically involved as double-counting with the decay topology  $pp \rightarrow q_H A_H, q_H \rightarrow q A_H$  could occur in specific parts of the parameter region and needs to be under precise control within the simulation. The detailed discussion of such a decay topology is postponed to a forthcoming study.

All simulations have been done automatically by `CheckMATE` using the event generator `MG5_aMC@NLO` and have been cross-checked with `WHIZARD`.

### 4.3 Scan Benchmark Scenarios

The LHT model —as already described earlier— depends on the following four parameters

1. the symmetry breaking scale  $f$  which affects the masses of all  $q_H, \ell_H, V_H$  and  $T^\pm$ .
2. the Yukawa parameter  $\kappa_q$  which affects the masses of the heavy quarks  $q_H$ ,
3. the Yukawa parameter  $\kappa_\ell$  which affects the masses of the color-neutral heavy fermions  $\ell_H$  and
4. the Yukawa parameter  $R$  which affects the masses of the heavy top partners  $T^+, T^-$ .

Furthermore we distinguish models in which a)  $T$ -parity is exactly conserved and b) models where gauge anomalies introduce the  $T$ -parity violating couplings  $A_H - W - W$  and  $A_H - Z - Z$ .

In order to reduce the number of free parameters we focus on particular benchmark scenarios with different theoretical and/or phenomenological motivation and with different assumptions on the fermion sector, the heavy top sector and the validity of  $T$ -parity. These scenarios result in  $3 \times 2 \times 2 = 12$  different benchmark cases, summarized in Tab. 2.

**Heavy Fermion Sector:** We first discuss the different assumptions on the heavy fermion sector. In the *Fermion Universality* model we set the two coefficients  $\kappa_q = \kappa_l$  equal and hence get a mass degeneracy in the heavy fermion sector. Due to their color charge, the production cross sections for processes involving heavy quarks are significantly higher than the respective cross sections for final states with color-neutral heavy fermions. Hence, we do not consider process 3 of our list in 4.1.

The masses of the heavy fermions have two important consequences for the phenomenology: they affect their production cross sections and they change the branching ratios of the heavy gauge bosons  $V_H \rightarrow \ell_H^{(*)} \ell'$ . To get an understanding which role this plays when setting bounds on the model we choose two further benchmark cases, each taking into account one of these effects.

In the *Heavy  $q_H$*  model we decouple the heavy quarks from the model by fixing  $\kappa_q = 3.0$ . This raises the heavy quark masses to the multi-TeV-scale and hence makes them experimentally inaccessible. Therefore, we do not consider production modes which involve

Sector	Model	Constraint	Phenomenology	Considered Topology
$f_H$	<i>Fermion Universality</i>	$\kappa_l = \kappa_q$	<ul style="list-style-type: none"> <li>• mass degeneracy of <math>q_H, \ell_H</math></li> <li>• <math>\ell_H</math> production negligible</li> </ul>	Exclude process 3
	<i>Heavy <math>q_H</math></i>	$\kappa_q = 3.0$	<ul style="list-style-type: none"> <li>• <math>q_H</math> decoupled</li> <li>• <math>\ell_H</math> production relevant</li> </ul>	Exclude processes 1, 2
	<i>Light <math>\ell_H</math></i>	$\kappa_l = 0.2$	<ul style="list-style-type: none"> <li>• <math>\ell_H</math> very light</li> <li>• <math>V_H</math> branching ratios change</li> </ul>	Exclude process 3
$T^\pm$	<i>Light <math>T^\pm</math></i>	$R = 1.0$	<ul style="list-style-type: none"> <li>• <math>T^\pm</math> are light/accessible</li> </ul>	Include process 4, 5
	<i>Heavy <math>T^\pm</math></i>	$R = 0.2$	<ul style="list-style-type: none"> <li>• <math>T^\pm</math> are heavy/inaccessible</li> </ul>	Exclude process 4, 5
$A_H$	<i>TPC</i>	No TPV	<ul style="list-style-type: none"> <li>• <math>A_H</math> is stable and invisible</li> </ul>	$A_H$ stable
	<i>TPV</i>	With TPV	<ul style="list-style-type: none"> <li>• <math>A_H</math> is unstable</li> </ul>	$A_H \rightarrow VV$ decays

**Table 2.** Definitions of the considered benchmark models of this study. In this work we consider all  $3 \times 2 \times 2$  combinations of the options given in this table. The process numbers refer to the list in Eq. (4.1).

$q_H$ , i.e. processes 1 and 2 of 4.1, but take into account  $\ell_H$  pair production, process 3, instead. The results of this benchmark scenario should give insight to which degree the LHC sensitivity relies on the presence of the color-charged objects and which limits can be determined from searches looking for color-neutral particles only.

The *Light  $\ell_H$*  benchmark is also designed to lift the degeneracy of the color-charged and color-neutral objects. Here, by fixing  $\kappa_\ell$  to a small value of 0.2, the latter are light enough for the heavy gauge bosons to decay into them. We are interested to see how this change in the expected decay patterns affects the bounds compared to the *Fermion Universality* model. Note that even though the  $\ell_H$  are light we do not take into account the bounds from  $\ell_H$  production as we are interested in how only a change in the decay pattern affects the resulting bounds. The bounds resulting from direct  $\ell_H$  production are determined in the previously discussed *Heavy  $q_H$*  benchmark.

The results of these three benchmark cases should be sufficient to qualitatively determine the resulting bounds for other  $\kappa_q - \kappa_\ell$  combinations and to avoid a full 3D parameter scan in the  $f - \kappa_q - \kappa_\ell$  plane.

**Heavy Top Partner Sector:** The main phenomenological difference between the heavy top partners  $T^\pm$  and the other heavy fermions  $q_H$  is that their mass depends on  $R$  instead of  $\kappa$ . We choose two benchmark values for this parameter in such a way that one results in experimentally accessible top partners ( $R = 1.0$ ) while the other ( $R = 0.2$ ) does not. The value  $R = 1.0$  also corresponds to a case where minimal fine-tuning can be achieved, see [19, 26], and thus this benchmark case tests the natural regions of parameter space of the LHT model. In the *Heavy  $T^\pm$*  scenario we ignore any processes which involve these particles as they are too heavy to result in an LHC exclusion. The comparison of the two bounds at  $R = 1.0$  and  $R = 0.2$  gives insight to which degree the masses of the particles in this sector are relevant for the overall sensitivity.

**$T$ -Parity Violation:** As discussed in Sec. 2.1, gauge anomalies in the heavy sector can result in anomalous  $T$ -parity violating  $A_H - W - W$  and  $A_H - Z - Z$  couplings. The presence of these operators may drastically change the expected collider phenomenology as the final state not necessarily contains an invisible particle any more. Supersymmetry motivated searches are however still expected to be sensitive as the leptonic decays of the  $W$  and the invisible decays of the  $Z$  boson can still produce a significant amount of missing energy. We are interested to see by how much the bounds derived for the  $T$ -parity conserving case are changed due to these anomaly-mediated decays. For that reason we analyze each of the above discussed benchmark scenarios once with a stable  $A_H$  and once with enabling  $A_H \rightarrow VV$  decays.

## 5 Collider Topologies

For the discussion of the LHC results, it is useful to understand both the values of the production cross sections for all the processes we listed in the last section and the dominant branching ratios of the relevant final state BSM particles. Collider bounds are expected to be set by processes with a large production cross section times a decay topology with only a small Standard Model contamination. In this section we review the parameter dependence of these observables in order to determine the theoretically expected collider topologies of our LHT benchmark scenarios. Many of them are relevant for the discussion of the exclusion bounds that we determine with **CheckMATE** in the upcoming section.

### 5.1 Cross Sections

We start with a discussion of the production cross sections for all the process sets listed in Sec. 4.2. In Figs. 1,2 we show the cross sections for  $\sqrt{s} = 13$  TeV as a function of the symmetry breaking parameter  $f$  with fixed  $\kappa$  and vice versa. As the benchmark case *Light*  $\ell_H$  does not affect any production mode, the cross sections are identical to those in the *Fermion Universality* benchmark. In all cases we show the results in the *Light*  $T^\pm$  subscenario for which the  $T^\pm$  are kinematically accessible and the cross sections would nearly vanish in the case of *Heavy*  $T^\pm$ . Note that  $\kappa$  refers to  $\kappa_q = \kappa_\ell$  in the *Fermion Universality* case and to  $\kappa_q (\neq \kappa_\ell)$  in the *Light*  $\ell_H$  scenario.  $T$ -parity violation does not play a role in the discussion of LHT particle production which is why we do not distinguish *TPC* and *TPV* here. Results for center-of-mass energies of 8 and 14 TeV are provided in App. A.

Since the mass of all heavy sector particles increases with  $f$ , the cross sections for all processes drop with increasing  $f$ .<sup>4</sup> Similarly, since the mass of the heavy fermions depends linearly on  $\kappa$ , the cross sections for producing these particles becomes smaller for larger values of this parameter. As both mass and couplings of the  $T^\pm$  only depend on  $f$  and the fixed parameter  $R$ , no dependence on  $\kappa$  can be seen.

Interestingly, even though the mass of the vector bosons  $V_H$  also depends on  $f$  only, their production cross sections show a small  $\kappa$ -dependence in the *Fermion Universality*

---

<sup>4</sup>Small fluctuations in the  $f$ -dependent  $q_H q_H$  production cross section are caused by numerical noise.

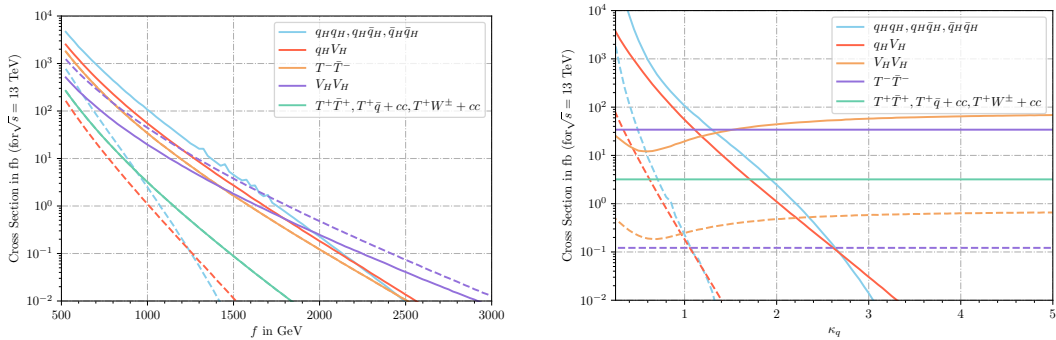


**Figure 1.** LHC production cross sections ( $\sqrt{s} = 13$  TeV) for benchmark models *Fermion Universality/Light  $\ell_H$  + Light  $T^\pm$* . Left: Dependence on  $f$  for fixed  $\kappa = 1.0$  (solid),  $\kappa = 2.0$  (dashed). Right: Dependence on  $\kappa$  for fixed  $f = 1$  TeV (solid),  $f = 2$  TeV (dashed). Labels in the legend appear in decreasing order of the respective maximum value of the solid lines.

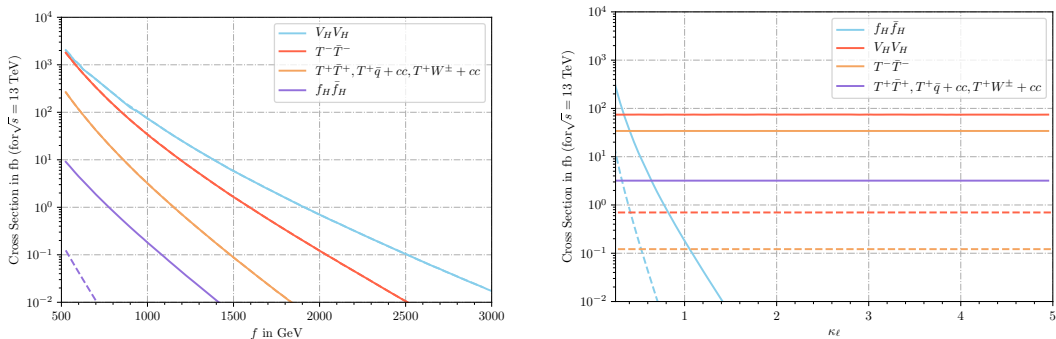


**Figure 2.** Same as Fig. 1 for benchmark model *Heavy  $q_H$  + Light  $T^\pm$* .

scenario. This is due to contributions of  $t$ -channel  $q_H$  which interfere destructively with the  $s$ -channel vector-boson diagrams. Since all masses scale linearly with  $f$ , this effect appears nearly independently of  $f$  at the position  $\kappa \approx 0.5$ . As a result, the cross section for  $V_H$  pair production is roughly a factor 5 smaller for small  $\kappa \approx 0.5$  than for large values  $\kappa \gtrsim 4$  when the heavy fermions are decoupled. As the  $q_H$  are by construction decoupled in the *Heavy  $q_H$*  benchmark scenario, the  $\kappa$  dependence of the  $V_H V_H$  production cross section vanishes in the resulting distribution shown in Fig. 2.

The production cross sections can reach values up to  $10^3$  fb and we thus expect the  $\sqrt{s} = 13$  TeV LHC to be sensitive to large regions of the parameter space we considered. Even for values of  $f \approx 3$  TeV, cross sections of order  $10^{-1}$  fb and thus detectable event rates can be expected which improves results from LHC Run 1 which were insensitive to values of the symmetry breaking scale above 2 TeV [19, 26]. Comparing the results of both the  $f$ - $\sigma$  and the  $\kappa$ - $\sigma$  planes, it becomes clear that there is no dominant process with a universally largest cross section. The cross sections have very different dependencies on  $\kappa$  and  $f$  and thus different regions in parameter space are expected to have different dominating final states.

Generally, regions with small values of  $\kappa$  and thus with light  $q_H, \ell_H$  predict a large



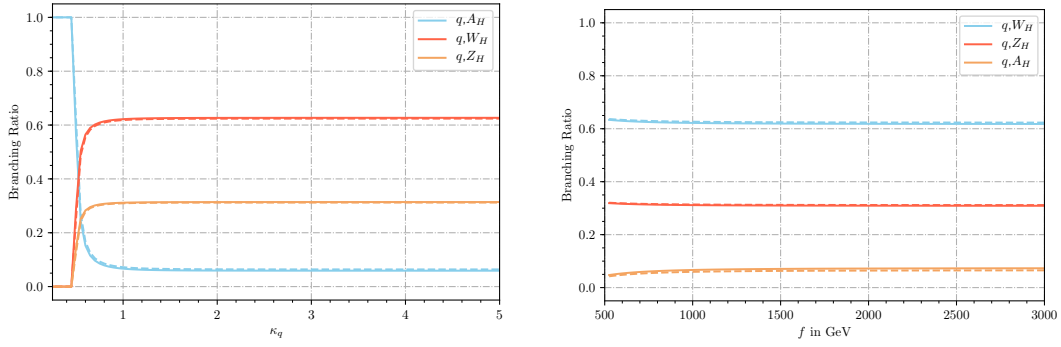


**Figure 3.** Branching ratios of  $d_H$  in the *Fermion Universality/Light  $\ell_H$*  model. Items in legend appear in decreasing order of the maximum value of the respective curve. Left: Fixed  $f = 1$  TeV (solid),  $f = 2$  TeV (dashed). Right: Fixed  $\kappa = 1$  (solid),  $\kappa = 2$  (dashed).

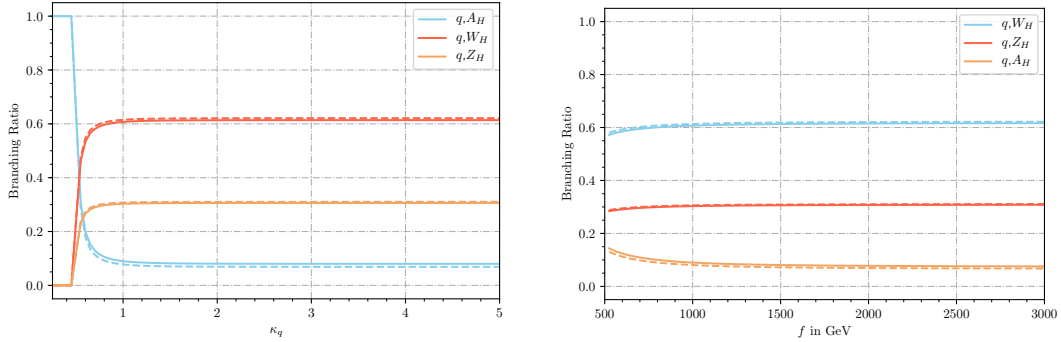


**Figure 4.** Branching ratios of  $u_H$  in the *Fermion Universality/Light  $\ell_H$*  model. Parameters as in Fig. 3.

rate of produced heavy fermions. As expected for a hadron collider, the  $q_H$  production is about two to three orders of magnitude larger than the production of heavy leptons  $\ell_H$  and the latter appear only to be relevant for small values  $f \lesssim 1$  TeV,  $\kappa \lesssim 0.5$ . In regions with larger values of  $\kappa$ , the production of heavy vector bosons becomes more important as their mass is independent of  $\kappa$ . If heavy top partners  $T^\pm$  are accessible, they are produced with comparable abundance as the heavy vector bosons.<sup>5</sup> Since the  $T^-$  is always lighter than the  $T^+$ , the production of the latter appears to be negligible in comparison.

## 5.2 Branching Ratios

We now continue with a discussion of the branching ratios for the relevant partner particles within the given benchmark cases. Note that we combine phenomenologically similar branching ratios which involve  $q := u, d, c, s$ , (so we particularly do not distinguish heavy up- and down-type quarks here)  $\ell = e, \mu, \tau$ ,  $\nu := \nu_e, \nu_\mu, \nu_\tau$  and their respective heavy part-

<sup>5</sup>Note that this statement in general depends on the specific value of the additional parameter  $R$  which we fixed to 1.0 in our benchmark scenario.

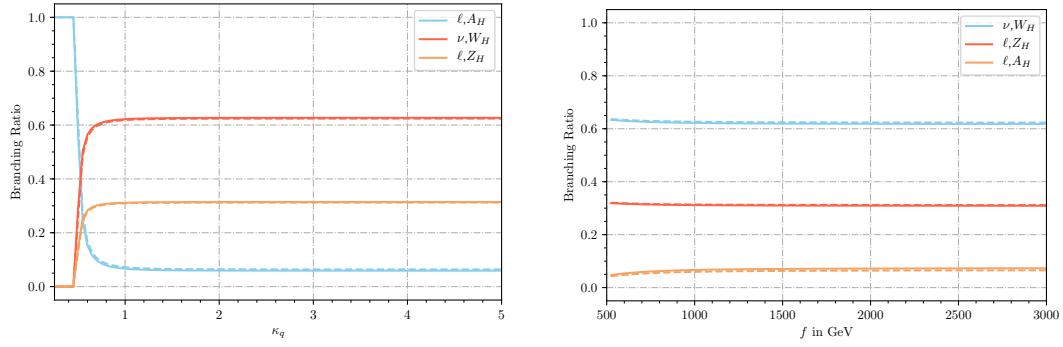


**Figure 5.** Branching ratios of  $\ell_H$  in the *Fermion Universality* model.

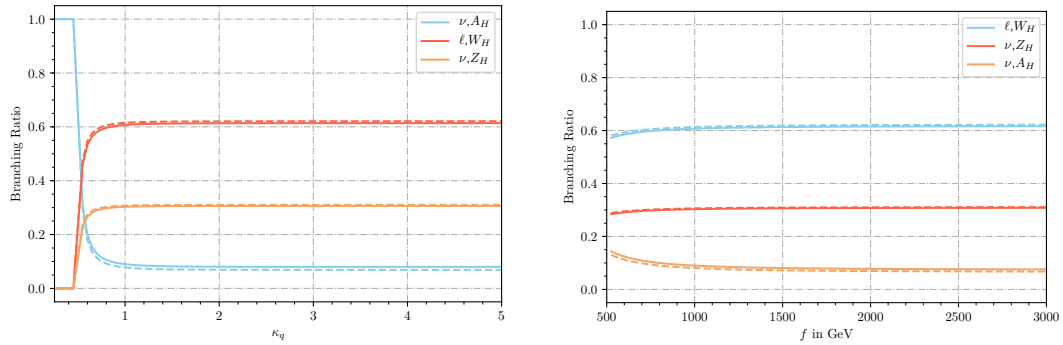


**Figure 6.** Branching ratios of  $\nu_{e,H}$  in the *Fermion Universality* model.

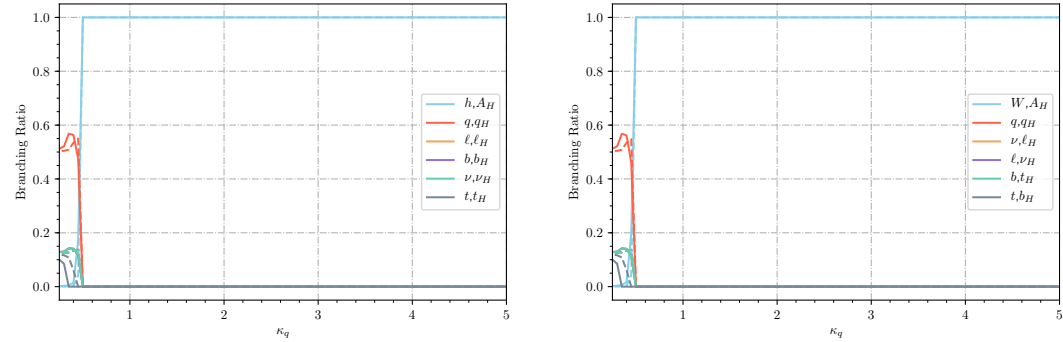


**Figure 7.** Branching ratios of  $Z_H$  (left) and  $W_H$  (right) in the *Fermion Universality* (The *Heavy  $q_H$*  scenario is very similar, cf. text). Parameters as in Fig. 3. In both plots, curves corresponding to decays with  $\nu, \ell$  or  $b$  are nearly identical.

ner fermions.<sup>6</sup> Also, we only discuss those decays with a branching ratio of at least 1 % anywhere in the discussed parameter space. Though we do not show it in the plots, we analytically calculated all decay widths and considered all kinematically allowed 2-body final

<sup>6</sup>It is only in this section where we distinguish between the charged heavy fermion  $\ell_H$  and the neutral particle  $\nu_H$ . In the rest of this work,  $\ell_H$  refers to both heavy charged and heavy neutral leptons.

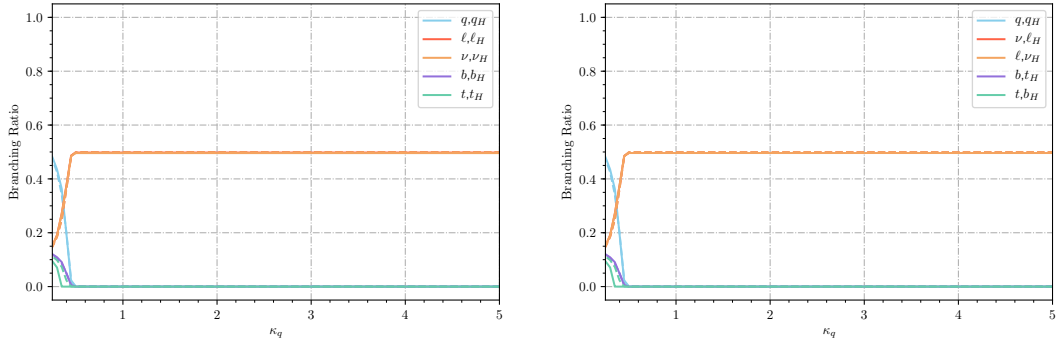


**Figure 8.** Branching ratios of  $Z_H$  (left) and  $W_H$  (right) in the *Light*  $\ell_H$  model.  $f$  is chosen as in Fig. 3, left. In both plots, the curves corresponding to decays with  $\nu$  or  $\ell$  are nearly identical.

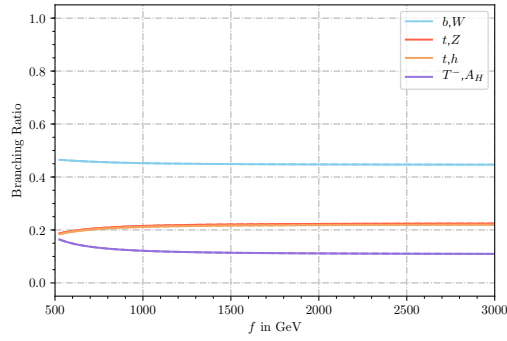


**Figure 9.** Branching ratios of  $T^+$  in the *Light*  $T^\pm$  scenario.

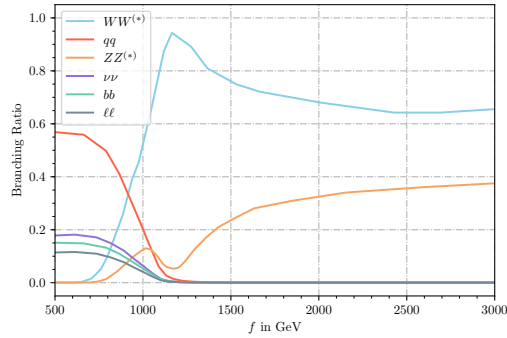


**Figure 10.** Branching ratios of  $A_H$  in the *TPV* benchmark.

states in the decay tables used in our scans in order to get correct values for the branching ratios. We mainly discuss results for the *Fermion Universality* and the *Light*  $\ell_H$  scenarios as the *Heavy*  $q_H$  scenario does not show any differences in the observable decay pattern - except for one difference which we mention along the way. Obviously, it is only the decay of the  $A_H$  which shows different behaviour in the benchmark cases *TPV* and *TPC*. These

two benchmarks are hence not distinguished in the discussion regarding the decays for the other particles.

Within the parameter ranges that we focus on, the particles  $T^-$ ,  $\ell_H$  and  $\nu_H$  each only have one decay mode in some scenarios:

$$\text{Light } T^-: \quad \text{BR}(T^- \rightarrow tA_H) = 1 \quad (5.1)$$

$$\text{Light } \ell_H: \quad \text{BR}(\ell_H/\nu_H \rightarrow \ell/\nu A_H) = 1 \quad (5.2)$$

For other particles and/or other scenarios there is more than one decay mode and the branching ratios depend on the values of  $f$  and/or  $\kappa$ .

In Figs. 3,4 we show the dominating branching ratios of the heavy quark partners  $d_H, u_H$ , respectively, in the *Fermion Universality/Light  $\ell_H$*  models which show identical results in this regard. As before, we show curves as functions of both  $\kappa$  and  $f$ . For both up- and down-type heavy quark partners, the decay into a heavy  $W_H$  boson and a quark is the most important decay with a branching ratio of nearly 60 % — whenever it is kinematically allowed. They are followed by decays into  $Z_H q$  of order 30 % and to  $A_H q$  of order 10 %. A small variation with  $f$  becomes visible which is caused by a subdominant dependence of the respective coupling constants on  $v/f$  (see e.g. [30]). This dependence differs between up- and down-type quarks and thus the variation with  $f$  differs for these two flavors. Note that very small values of  $\kappa_q \lesssim 0.5$  lead to  $m(q_H) < m(W_H), m(Z_H)$  and thus forbids decays  $q_H \rightarrow (W/Z)_H + X$ . All  $q_H$  therefore decay to the light  $A_H$  in this region of parameter space.

Note that due to the overall mass degeneracy and the identical quantum numbers within the *Fermion Universality* model, the decay signatures of all other heavy fermions, except for the  $T^\pm$ , are identical after replacing the corresponding up- and down-type components of the respective SU(2) doublets. For example, the branching ratio for  $\nu_{eH} \rightarrow W_H e$  is identical to the branching ratio  $u_H \rightarrow W_H d$ , see Figs. 3-5.

Next, we discuss the decays of the heavy gauge bosons  $W_H$  and  $Z_H$  for the *Fermion Universality* model in Fig. 7 and for the *Light  $\ell_H$*  model in Fig. 8. We only show results depending on  $\kappa$  as there is no  $f$  dependence for the two standard benchmark values  $\kappa = 1.0, 2.0$  which we considered. In case of *Fermion Universality*, the decay  $V_H \rightarrow f_H f'$  into a heavy fermion partner is only allowed for  $\kappa \lesssim 0.5$  and in this region decays into heavy quarks dominate. For larger values of  $\kappa$ , the only available decays are  $W_H \rightarrow W A_H$  and  $Z_H \rightarrow h A_H$ . In the *Light  $\ell_H$*  scenario, this picture changes by construction: the  $\ell_H$  are fixed to light masses and thus for  $\kappa_q \gtrsim 0.5$  both heavy gauge bosons decay to 50 % into  $\ell_H \ell$  and  $\nu_H \nu$ . Again, for smaller values of  $\kappa_q$  decays into  $q_H$  are kinematically accessible and have a dominant branching ratio. The branching ratio curve for the benchmark scenario *Heavy  $q_H$*  corresponds to the one for *Fermion Universality* with the only exception that the decay  $V_H \rightarrow q_H q$  disappears for  $\kappa < 0.5$  and the branching ratios for the other modes scale up accordingly.

In Fig. 9 we show the branching ratios of the heavy top partner  $T^+$  (note that  $T^-$  always decays to  $tA_H$  as listed above) in the *Light Top* benchmark, i.e. for  $R = 1.0$ . As  $T^+$  is a  $T$ -parity even particle it must decay into pairs of  $T$ -odd particles or purely into

SM particles. This results in four main decay scenarios. The SM decays follow mainly the pattern of a  $SU(2)_L$  singlet top partner (cf. e.g. [54]) of 50 % branching ratio into  $bW^+$  and equally a quarter into  $th$  and  $tZ$ . This is only slightly modified by the only accessible  $T$ -odd particle decay, namely roughly 15 % branching ratio into  $T^- A_H$ . The changes the top-like decay into  $bW^+$  into nearly 45 % branching ratio, while  $th$  and  $tZ$  have roughly 20 % branching ratio each. These branching ratios have no dependence on  $\kappa$  and only little dependence on  $f$  which originates from the  $f$ -dependence of the  $T^\pm$  and  $A_H$  masses.

We finish the discussion with the branching ratios of the  $A_H$  in the  $TPV$  scenario shown in Fig. 10, which only depend on  $f$ . The information shown in this figure has been taken from a detailed calculation performed in Ref. [18]. One observes that for  $f > 1200$  GeV, decays into on-shell Standard Model gauge boson pairs dominate. For smaller values of  $f$ , the  $A_H$  mass drops below 180 GeV, the partial decay widths into gauge bosons decrease due to kinematic suppression and the loop-induced decays into Standard Model leptons become equally relevant. For  $f \lesssim 900$  GeV,  $A_H$  decays predominantly into SM quark pairs.

### 5.3 Expected Final State Topologies and Correspondence to Supersymmetric Searches

In this section we combine the information of the preceding one with the list of dominant production processes given in Sec. 4.2 in order to find the following expected final state signatures. Comparing them to the specialized analyses of the experimental collaborations for supersymmetry, we can make the following classification of the signatures and their applicability to the LHT model:

- In general – if  $T$ -parity is conserved – all  $T$ -odd particles produce decay chains with a stable  $A_H$  as the lightest  $T$ -odd particle at the end. This particle is experimentally invisible and thus produces missing transverse momentum  $\cancel{E}_T$  in the event. This is in close analogy to  $R$ -parity conserving supersymmetry which produces decay chains with the lightest neutralino at the end which similarly produces  $\cancel{E}_T$ . Therefore, many searches looking for  $R$ -parity conserving supersymmetry require  $\cancel{E}_T$  in the event and thus are sensitive to our model.
- Final states with heavy gauge bosons  $W_H, Z_H$  behave differently in the main benchmark cases. In the *Fermion Universality* model, where  $W_H$  decays produce  $W$  bosons which either contribute with further jets in their hadronic decays or with further hard leptons in their leptonic decays, the heavy  $Z_H$  adds Higgs bosons in the final state which mainly lead to additional  $b$ -jets in the event. This final state topology is thus similar to supersymmetric electroweakino production  $\tilde{\chi}_1^\pm \tilde{\chi}_2^0 + \tilde{\chi}_1^\pm \tilde{\chi}_1^\pm + \tilde{\chi}_2^0 \tilde{\chi}_2^0$  with a Wino-like chargino and a Higgsino-like neutralino.

In the *Light Leptons* model, the heavy gauge bosons almost always decay into a lepton and the corresponding heavy lepton partner which itself always decays into a lepton and  $A_H$ . This behavior corresponds to a supersymmetry model with very light scalar leptons for which there exist specific signal regions in experimental searches for electroweakinos.

- Final states with heavy  $q_H$  always produce quarks and  $A_H$  in their decays and hence result in final states with jets and missing transverse momentum. In most cases these decays produce further heavy gauge bosons  $V_H$  which, as explained above, add more leptons,  $b$ -jets or normal jets to the event. This topology is very similar to supersymmetric scalar quark production with either direct decays into the lightest supersymmetric particle or with decay chains producing further neutralinos and/or charginos in the final state.
- Final states with the  $T$ -odd  $T^-$  produce final states with SM tops and missing transverse momentum, a typical signature of natural supersymmetry with a light scalar top.
- Final states with the  $T$ -even  $T^+$  not necessarily produce missing transverse momentum but instead decay top-like into  $bW^+$ , hence are expected to affect SM top measurements, or decay into top + Higgs/gauge boson final states which is a typical feature of models with an extended quark sector. Since processes involving  $T^+$  have a reduced production cross section, see our earlier discussion, and since our searches mostly focus on SUSY-like final states, we do not expect these particles to be of great relevance for our results.
- If  $T$ -parity is violated by small couplings, we still expect the same production and decay topologies as in the  $T$ -parity conserving case which typically produce 2  $A_H$  and the same hard final state objects which we listed in the previous discussion. However, as now each of these decays into pairs of Standard Model particles, many more final state topologies appear. Especially if  $f \gtrsim 1.2 \text{ TeV}$  we expect four Standard Model vector bosons in the final state and as each of these can decay hadronically or leptonically, a plethora of possible final state exists with various combinations of additional jets and leptons. These can be covered by analyses which target very large final state multiplicities for which the Standard Model background is very small. Furthermore, as both  $Z$  and  $W$  have sizable decay rates into final states with neutrinos, the final states may even have a significant amount of missing transverse momentum and thus may still be covered by the same supersymmetry-based analysis strategies as mentioned for the  $T$ -parity conserving case.

All in all we expect various final states which are very similar to those expected in typical supersymmetric models and we expect that this model can be strongly constrained by applying LHC searches originally designed to find supersymmetric particles. Even though theoretically expected, some of these topologies not necessarily will result in a large enough signal event rate to produce a sensible bound and/or various topologies appear simultaneously and it is difficult to say *a priori* which of these topologies is expected to result in the strongest sensitivity. Fortunately, as many of these searches are implemented in the tool **CheckMATE**, we expect this tool to perform very well in our scenarios and determine the respectively strongest bounds for each benchmark case conveniently. However, not all conceivable topologies mentioned here have a matching analysis implemented in **CheckMATE** and therefore most sensitive topologies determined below might not necessarily correspond

CM identifier	Final State	Designed for	Ref.
atlas_conf_2016_096	$\cancel{E}_T + 2\text{-}3 \ell$	$\tilde{\chi}^\pm, \tilde{\chi}^0, \tilde{\ell}$	[55]
atlas_conf_2016_054	$\cancel{E}_T + 1 \ell + (\text{b})\text{-j}$	$\tilde{q}, \tilde{g}$	[56]
atlas_conf_2017_022	$\cancel{E}_T + 0 \ell + 2\text{-}6 \text{j}$	$\tilde{q}, \tilde{g}$	[57]
atlas_conf_2017_039	$\cancel{E}_T + 2\text{-}3 \ell$	$\tilde{\chi}^\pm, \tilde{\chi}^0, \tilde{\ell}$	[58]

**Table 3.** Small summary of all  $\sqrt{s} = 13$  TeV analyses which appear in the discussion of our results. More details, also on other tested analyses, are given in Tab. 5 in the appendix.

to what we theoretically expect at this stage. Our previous discussion should hence be understood as a more general summary of interesting LHC topologies worthwhile investigating at the Large Hadron Collider out of which we cover a large fraction with our following CheckMATE analysis.

## 6 Collider Results from CheckMATE

We now discuss the results of our collider analysis performed with CheckMATE. Exclusion lines in the  $\kappa$ - $f$ -plane for all  $3 \times 2 \times 2$  scenarios are shown in Figs. 11-22. For each case, we choose two ways to present our results. On the respective plots in the left column we show the total exclusion line determined by CheckMATE from LHC analyses at 8 TeV and 13 TeV, respectively. The 8 TeV results allow direct comparison to earlier studies, e.g. in [19, 26]. Drawing them in the same plot with the updated 13 TeV results illustrates how the increased energy and the higher integrated luminosities significantly improve the sensitivity on the Little Higgs Model with fully or nearly conserved  $T$ -parity. In the discussion in the main text of this section we focus on the update from the current results at  $\sqrt{s} = 13$  TeV and will not discuss the outdated results at 8 TeV center-of-mass energy. In the same set of plots we also show mass contours of the most relevant particles to understand the bounds. These are

- the heavy gauge boson mass  $Z_H$  ( $= W_H$ ),
- the heavy quarks  $q_H$  for all models except *Heavy*  $q_H$ ,
- the heavy leptons  $\ell_H$  for the model *Heavy*  $q_H$ ,
- the  $T$ -odd heavy top partner  $T^-$  mass for *Light*  $T^\pm$  benchmarks and
- the heavy photon mass  $A_H$  for *TPV* models.

To keep the plots readable we do not show all contours in all plots. With the exception of  $T^\pm$  whose mass values are only meaningful in the *Light*  $T^\pm$  scenario, all plots with same heavy fermion sector scenario (see Table 2) have the same particle spectrum and therefore, each iso-mass contour can be understood to appear in all other plots of the same main benchmark scenario.

Alongside the above results we show a second plot each for all benchmark scenario where we focus on the experimental signature(s) which lead to the overall bound. For each

benchmark study, we show the respective **CheckMATE** analyses which cover the excluded region at  $\sqrt{s} = 13$  TeV. The names in the legend correspond to the **CheckMATE** analysis identifiers and we provide a small summary of their respective covered topologies in Tab. 3 for convenience. Note that regions with small  $\kappa$  and small  $f$  are typically covered by many more LHC analyses but we only show the minimal set of analyses sufficient to cover the entire excluded region. A full list of all **CheckMATE** analyses that we considered for this study can be found in Tab. 5 in the appendix B.

## 6.1 Fermion Universality

We start with a discussion of the *Fermion Universality* model in which the heavy fermion Yukawa couplings are set to be equal,  $\kappa_q = \kappa_\ell$ , and thus features a degenerate spectrum of heavy quarks and heavy leptons.

### *T*-parity conserved and heavy $T^\pm$

In Fig. 11 we start with the subscenario of conserved *T*-parity and with the heavy top sector decoupled. The excluded parameter spaces can be separated into two main regions:

- For large  $f \geq 1$  TeV, the exclusion line depends both on  $\kappa$  and  $f$  and runs nearly parallel to the iso-mass contours of the heavy quarks. It thus nearly follows the inequality  $f \times \kappa < f\kappa_{\max}$  with  $f\kappa_{\max} \approx 1.5$  TeV at  $\sqrt{s} = 8$  TeV and  $\approx 2$  TeV at  $\sqrt{s} = 13$  TeV. The most sensitive analysis looks for at least two hard jets and a large amount of missing transverse momentum, a topology which in this region appears through heavy quark pair production with each heavy quark decaying into a quark, an invisible heavy photon and possible additional particles via more complicated cascades in the decay,  $q_h q_H \rightarrow qq A_H A_H + X$ . The expected event rate for this QCD-induced process mainly depends on the mass of the heavy quarks and thus explains why the bound runs nearly parallel to the  $q_H$  iso-mass contours. Still, *t*-channel heavy vector bosons also have a small effect on the production cross section and thus the bound drops slightly faster with higher  $f$ , i.e. with larger  $m(V_H)$ , than the  $m(q_H)$  iso-mass contour. The results translate into a bound on  $m_{q_H}$  of  $\geq 3$  TeV for  $f \approx 1$  TeV which decreases to  $m_{q_H} > 2$  TeV for  $f \gtrsim 3$  TeV.
- For smaller values of  $f$ , the bound becomes nearly independent of the specific values of  $f$  or  $\kappa_q$  and absolutely excludes  $f > 900$  GeV. For large enough values of  $\kappa$ , the heavy quarks are not created abundantly enough and hence we are only sensitive to the electroweak production of heavy gauge bosons  $V_H$  whose mass is independent of  $\kappa_q$ . The given limit can then be interpreted as an absolute mass bound  $m_{Z_H} = m_{W_H} \gtrsim 600$  GeV. Even though their mass is  $\kappa$ -independent, the bound still becomes stronger for increasing value of  $\kappa_q$ . This is — see our discussion in Sec. 5.1 — due to  $\kappa_q$  affecting the mass of the heavy quarks who in turn interfere destructively with their contribution to the total  $V_H V_H$  production cross section. Thus the weakest bound  $f > 800$  GeV appears for  $\kappa_q \approx 2.5$  and improves to  $f \gtrsim 950$  GeV for  $\kappa \gtrsim 5.0$ .

Interestingly, even though the main production channel has changed, the most sensitive study is the same multijet analysis as before. The required topology is created



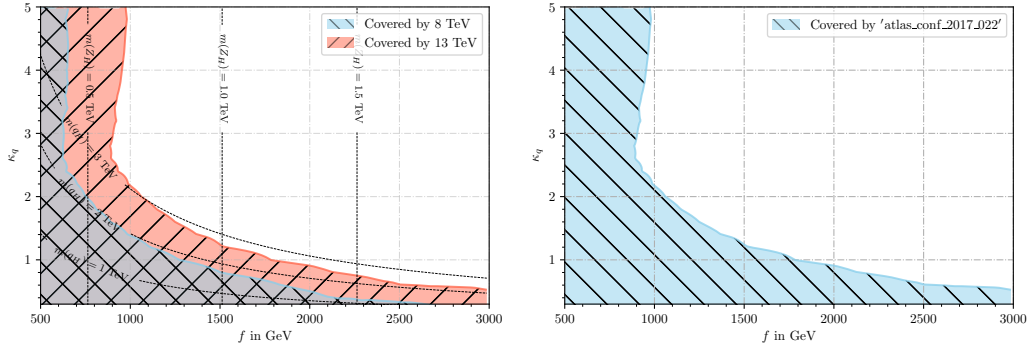


Figure 11. Results for scenario  $(Fermion\ Universality) \times (Heavy\ T^\pm) \times (TPC)$

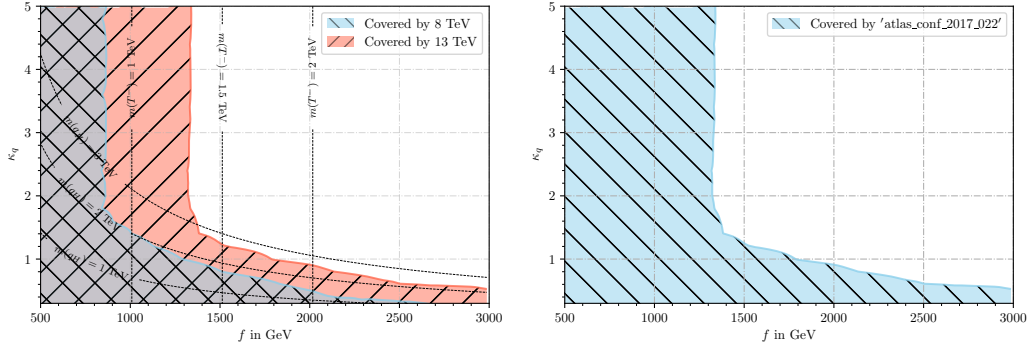


Figure 12. Results for scenario  $(Fermion\ Universality) \times (Light\ T^\pm) \times (TPC)$

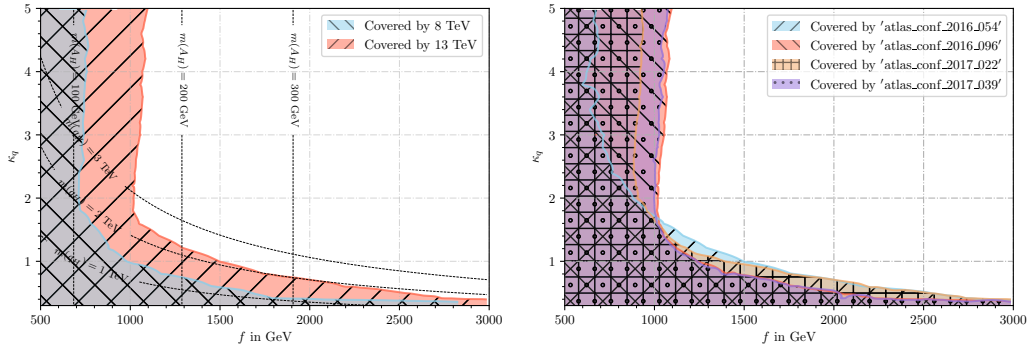


Figure 13. Results for scenario  $(Fermion\ Universality) \times (Heavy\ T^\pm) \times (TPV)$

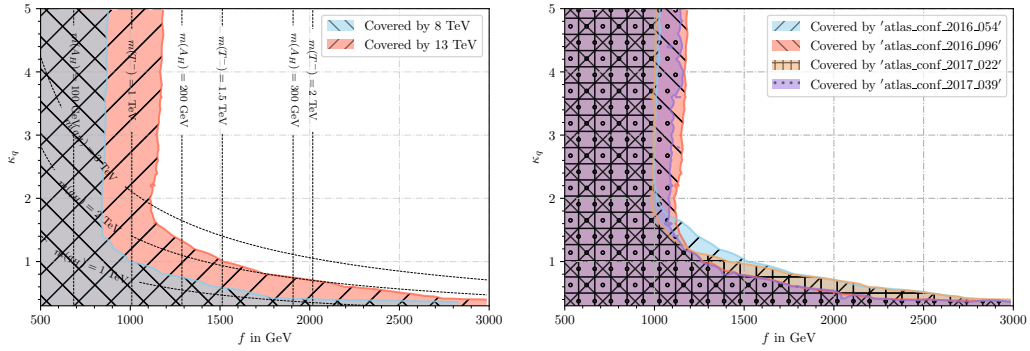


Figure 14. Results for scenario  $(Fermion\ Universality) \times (Light\ T^\pm) \times (TPV)$

from hadronically decaying  $W$ -bosons in  $W_H \rightarrow WA_H$  and from  $b$ -jets in the decay to a Higgs boson of  $Z_H \rightarrow hA_H$ .

### $T$ -parity conserved and light $T^\pm$

To see how the sensitivity to the heavy top partners compares to the previous bound, we show below in Fig. 12 the results of the same model, but now with  $R = 1.0$  and thus including processes which involve the production of heavy  $T^\pm$ . Note that for fixed  $R$ , the mass of the  $T^\pm$  only depends on  $f$  which is why for large  $f$  these particles are not experimentally accessible. Thus, we get the same bound on  $(f\kappa_{\max})$  as explained for the previous benchmark.

However, if the  $T^\pm$  are kinematically accessible they play an important role for the overall bound. For our special case with  $R = 1.0$ , we observe that the absolute bound on  $f$  increases to  $f \geq 1.3$  TeV and becomes entirely  $\kappa$  independent as the  $T^\pm$  production modes, as opposed to the  $V_H$  modes discussed before, do not depend on the heavy quark sector. Again, we observe the search for multijets plus missing transverse momentum to be most sensitive for the bound.<sup>7</sup>

Clearly, the precise value of the lower limit on  $f$  depends on the mass of the heavy top partner particles which implicitly depends on the value of  $R$ . We emphasize here that the choice  $R = 1.0$  just serves as a benchmark case and any other  $R$  value would directly affect the bound, see Eq. (2.16), in either direction. We chose  $R = 1$  here for the reason that it is rather special as it minimizes the LHT contributions to the EWPO, cf. Sec. 3. Our more general conclusion from this benchmark study is thus that searches for  $V_H$  and for  $T^\pm$  can yield competitive absolute lower bounds on  $f$ , and while the bound derived from  $V_H$  production is nearly independent of the chosen benchmark, the presence of light top partners may put further constraints on the model.

### $T$ -parity violated

In Figs. 13, 14 we show the results in case we include the anomaly-mediated decays of the heavy photon  $A_H$  into vector boson or lepton pairs, both without (Fig. 13) and including (Fig. 14) the heavy top sector. We again split the discussion into the two main parameter regions already discussed before:

- We again observe a  $\kappa$ -dependent bound for large values of  $f$  which follows the iso-mass contour of the heavy quarks. However, compared to the  $T$ -parity conserving case the bound is now slightly weaker,  $m_{q_h} \geq 2.5$  TeV for  $f \approx 1$  TeV and  $m_{q_h} \geq 1.5$  TeV for  $f \approx 3$  TeV. There are two analyses with nearly identical sensitivity in this region, namely the already discussed zero-lepton–multijet plus  $\cancel{E}_T$  analysis and the related multijet analysis which requires one lepton in the final state. The fact that their sensitivity is fairly similar can be qualitatively understood from the fact that we

---

<sup>7</sup>Note that by the time this work was completed, the restricted set of analyses implemented in **CheckMATE** contained the updated multijet results with an integrated luminosity of  $36 \text{ fb}^{-1}$ , but had only searches for scalar tops implemented which use data from  $13.3 \text{ fb}^{-1}$ . This may explain why we observe multijet final states to be most sensitive even though in Sec. 5.3 we expected heavy top partners to produce distinct decay signatures which mimic scalar top decays in natural supersymmetry.

expect many additional final state gauge bosons which produce additional leptons and/or jets. Thus, both multijet studies with and without leptons become sensitive and we get an overall similar signal event rate in the respective signal regions of these two studies. In fact, as the branching ratio to  $WW$  increases for smaller  $f$ , see Fig. 10, and as  $W$ -bosons produce on average more charged leptons than  $Z$ -bosons, we expect analyses which require a final state lepton to become slightly more sensitive for smaller  $f$  — a feature which we exactly observe in our results in Fig. 13, on the right hand side.

At first, it appears unexpected that the bound is not significantly weakened, even though the originally invisible  $A_H$  now decays into Standard Model particles and thus appears to remove crucial missing transverse momentum from the event. However, one should bear in mind that we expect four additional boosted gauge bosons, two from each  $A_H$ , in the final state. Thus we expect to pass the  $\cancel{E}_T$  constraints if at least one of these decays into neutrinos. Even though on average the branching ratio  $V \rightarrow \nu + X$  is only around 25%, as we have four gauge bosons the probability of having an  $A_H A_H$  pair decaying into at least one neutrino and thus producing  $\cancel{E}_T$  is above 70%. This reduces the  $\cancel{E}_T$  cut acceptance slightly but not drastically compared to the  $T$ -parity conserving case. Furthermore, we get the same visible final state objects as in the  $T$ -parity conserving case, together with additional boosted particles from the gauge boson decays which may even improve the final state acceptance. It thus can be understood why the sensitivity does not drop significantly if  $T$ -parity violation is considered.

- Similarly to before, for a symmetry breaking scale  $f$  of the order 1 TeV we observe a  $\kappa$  independent bound. Interestingly, the bound has even improved after turning on  $T$ -parity violation and excludes  $f \gtrsim 1$  TeV for  $\kappa \approx 1.5$  and  $f \gtrsim 1100$  GeV for  $\kappa \approx 4.0$ . To understand why the limit becomes stronger one needs to look at the analysis coverage map on the right of Fig. 13. We see that the bound derived from the multijet analysis, which was most sensitive in the  $T$ -parity conserving case, slightly weakened. This can be understood with the same arguments as given before for the large- $f$  region. However, we also observe that the sensitivity is now dominated by electroweakino-motivated searches, more specifically by analyses which look for final state leptons and missing transverse momentum. A more detailed look in the results of that analysis reveals that it is in fact the signal region **SR-Slep-e** which produces the bound. This signal region requires 3 high- $p_T$  charged leptons which do not originate from a leptonically decaying  $W$ - $Z$ -pair and a significant amount of missing transverse momentum. Interestingly, such a signature could not be reached in the previous  $T$ -parity conserving benchmark case, because the most important topology  $pp \rightarrow W_H W_H \rightarrow WW A_H A_H$  only produces two leptons. Including  $T$ -parity violation, we can get a third, highly energetic lepton if one of the four final state gauge bosons is a leptonically decaying  $W$ . Furthermore, since this signal region has no constraints on the final state jet multiplicity, the decays of the other three gauge bosons is irrelevant. As such, a large signal event rate is expected for this analysis if

$T$ -parity is violated.

If the top partners are kinematically accessible, see Fig. 14, the absolute bound on  $f$  only increases slightly by about 100 GeV. The electroweak search stays the most sensitive analysis for this model. The resulting bounds increase as more events from the topology  $pp > T^-\bar{T}^- \rightarrow (bW)(bW)WWVV$  are expected. Again, the impact on the bound depends on the precise value of  $R$  and we only show one example here which illustrates that the details of the heavy top partner sector are relevant for the overall LHC limit.

Interestingly, the multijet analysis does not seem to get a significant contribution from the presence of the  $T^\pm$  even though it did in the previous case when  $T$ -parity was conserved, cf. Figs. 15, 16. To understand this behavior one needs to consider the details of the experimental search: this analysis tries to cover various hierarchies and decay topologies that can appear in the supersymmetric squark-gluino  $\tilde{g}, \tilde{q}$  sector and defines many signal regions which target different jet multiplicities. Different mass scales in the supersymmetric sector are taken into account by gradually increasing the requirements on the sum of jet  $p_T$  in the event as well as the total amount of  $\cancel{E}_T$ , more specifically by using cuts which require minimum values for the ratio  $\cancel{E}_T/\sum(\text{jet } p_T)$ . In supersymmetry, jet multiplicity, total hadronic energy and missing transverse momentum increase simultaneously as heavier particles on average produce longer decay chains and give more momentum to the visible jets and the invisible neutralino and thus a cut on  $\cancel{E}_T/\sum(\text{jet } p_T)$  has a good signal acceptance in supersymmetry.

However, such a cut is disadvantageous for our most important topology  $T^\pm \rightarrow tA_H$  if  $A_H$  decays via TPV: the additional decay of  $A_H$  into gauge bosons is expected to produce a significantly larger amount of jets and hadronic energy while reducing the amount of missing transverse momentum, resulting in a large drop in the signal acceptance. Therefore adding the  $T^\pm$  to the experimentally accessible spectrum hardly increases the amount of signal events in this case and the bound only improves little.

## 6.2 Heavy $q_H$

We continue with the discussion of the results for the *Heavy  $q_H$*  scenario which fixes  $\kappa_q$  to 3.0 and thus effectively decouples the  $q_H$  from the experimental reach. The results for all subscenarios (with/without  $T$ -parity violation and ex-/including the heavy top partner sector) are shown in Figs. 15-18. The plots show the same information as in the previous section 6.1, however note that the ordinate is now chosen to be the free parameter  $\kappa_\ell$  and the iso-mass contours are given for the  $\ell_H$  instead of the  $q_H$  now.<sup>8</sup>

To understand how the bounds change compared to the previous benchmark scenario, it is worth repeating the two main phenomenological consequences of this benchmark case:

1.  $q_H \rightarrow qV_H$  topologies are replaced by  $\ell_H \rightarrow \ell V_H$ . Multijet final states are thus replaced by multilepton final states. As the production cross section for  $\ell_H\ell_H$  is 2

---

<sup>8</sup>As the mass of the  $\ell_H$  and  $q_H$  are identical for  $\kappa_q = \kappa_\ell$ , see Eq. (2.22), the iso-mass contours for  $\ell_H$  appear at the same position as those for  $q_H$  in the previous benchmark.

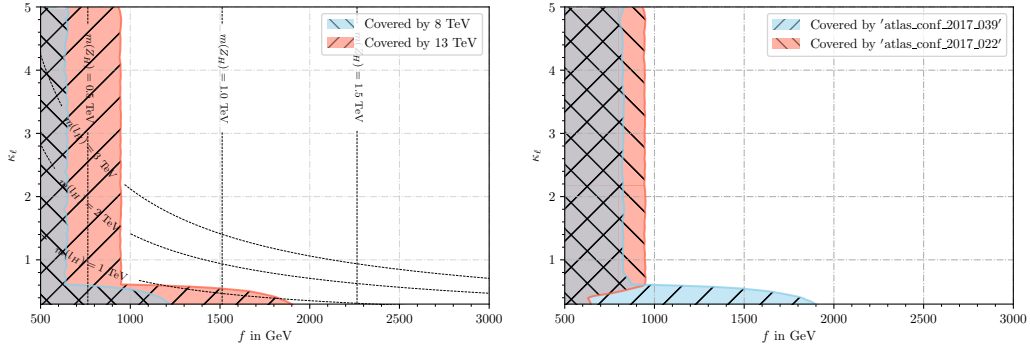


Figure 15. Results for scenario  $(Heavy\ q_H) \times (Heavy\ T^\pm) \times (TPC)$

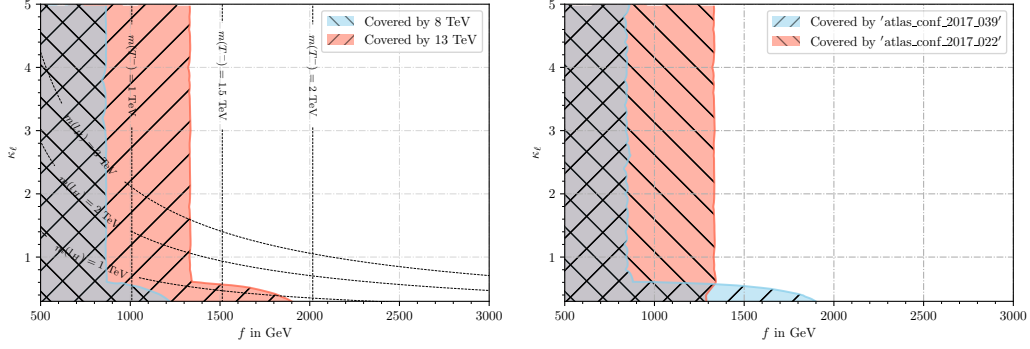


Figure 16. Results for scenario  $(Heavy\ q_H) \times (Light\ T^\pm) \times (TPC)$

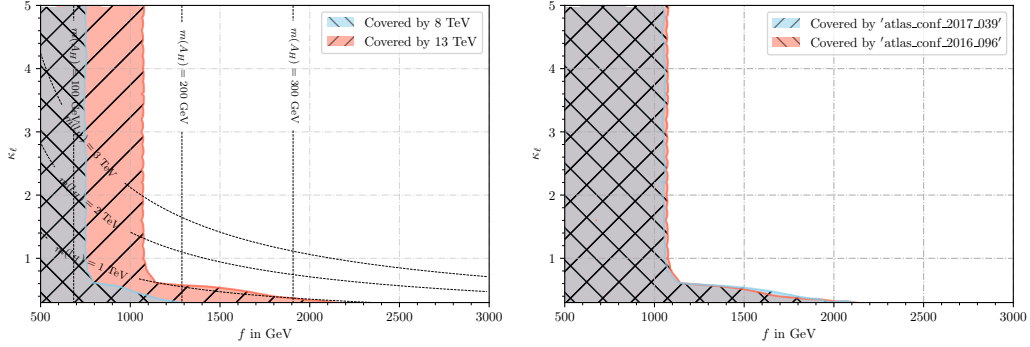


Figure 17. Results for scenario  $(Heavy\ q_H) \times (Heavy\ T^\pm) \times (TPV)$

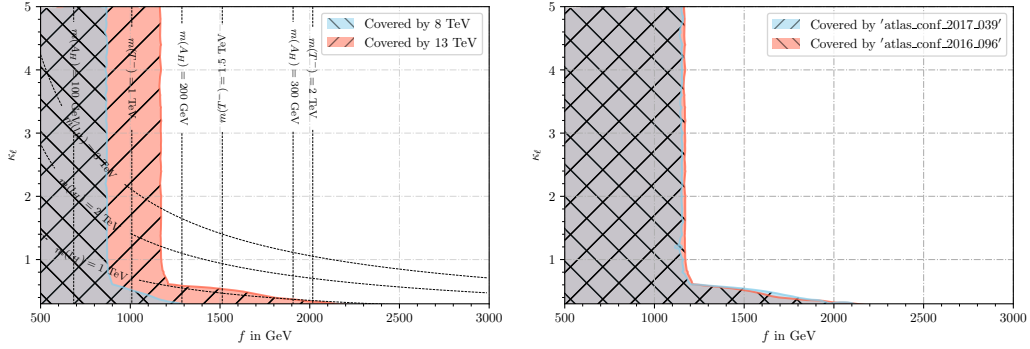


Figure 18. Results for scenario  $(Heavy\ q_H) \times (Light\ T^\pm) \times (TPV)$

to 3 orders of magnitude smaller than the corresponding cross section for  $q_H q_H$ , we expect a far weaker sensitivity in the heavy fermion dominated region (i.e. large  $f$ , small  $\kappa$ ).

2.  $\sigma(pp \rightarrow V_H V_H)$  was dependent on  $\kappa$  but is independent of  $\kappa_\ell$  as no contributions from  $t$ -channel  $q_H$  exist in this benchmark case. Thus we expect the bounds produced from  $V_H$  pair production to be entirely  $\kappa_\ell$  independent and very similar to the case  $\kappa = 3.0$  of the previous benchmark.

With these pieces of information in mind, the results in Figs. 15-18 compare straightforwardly to the bounds of the earlier benchmark scenario in Figs. 11-14:

- For  $f \approx 1$  TeV, vector boson production and potential heavy top partner production are the most sensitive channels and they produce  $\kappa_\ell$  independent bounds of  $f \gtrsim 950$  GeV (TPC, no  $T^\pm$ ),  $f \gtrsim 1350$  GeV (TPC, with  $T^\pm$ ),  $f \gtrsim 1100$  GeV (TPV, no  $T^\pm$ ) and  $f \gtrsim 1200$  GeV (TPC, with  $T^\pm$ ). The bounds correspond to those for the previous benchmark for large values of  $\kappa \gtrsim 4.0$ . The most dominant topologies also do not change: we observe multijet final states to be the most sensitive ones in case  $T$ -parity is conserved while multilepton final states become more important if  $T$ -parity is violated.
- For  $\kappa_\ell \lesssim 0.5$ , the mass of the  $\ell_H$  drops below the mass of the heavy vector bosons and thus decays of type  $V_H \rightarrow \ell_H \ell$  can happen, see Fig. 7. The boosted final-state leptons of this decay can be observed via a multilepton analysis as can be seen in the right of Fig. 15. This significantly improves the sensitivity and improves the bound on  $f$  to up to 1.9 TeV. As the branching ratios depend on  $\kappa$ , this bound is now slightly dependent on  $\kappa$ .
- The “ $f_{\kappa_{\max}}$ ”-bound which we were able to set in the previous benchmark almost disappears for this scenario where the  $q_H$  are decoupled. The expected event rates from  $\ell_H \ell_H$  pair production are so small that no feasible bound can be set from this topology in case of  $T$ -parity conservation, even with the newest  $\sqrt{s} = 13$  TeV results. It is only in the case of  $T$ -parity violation that we can observe an exclusion for very small values of  $\kappa$  which follows the  $m(\ell_H) = 1$  TeV mass contour, caused by a slight increase of the expected multilepton event rates from leptonic gauge boson decays, see our discussion above.

All in all we observe that the presence or absence of the  $q_H$  partner particles plays a very important role for determining the LHC limits in the low  $\kappa$  region, i.e. for  $\kappa \lesssim 1.5$ . However, the heavy gauge boson sector also puts very important constraints on  $f$  and as the collider phenomenology of this sector is almost, but not completely, independent of the heavy fermion sector, the absolute bounds on  $f$  are very robust against choices for the heavy quark sector. In fact, they tend to become stronger as the presence of light  $q_H$  decreases the  $V_H V_H$  production cross section.

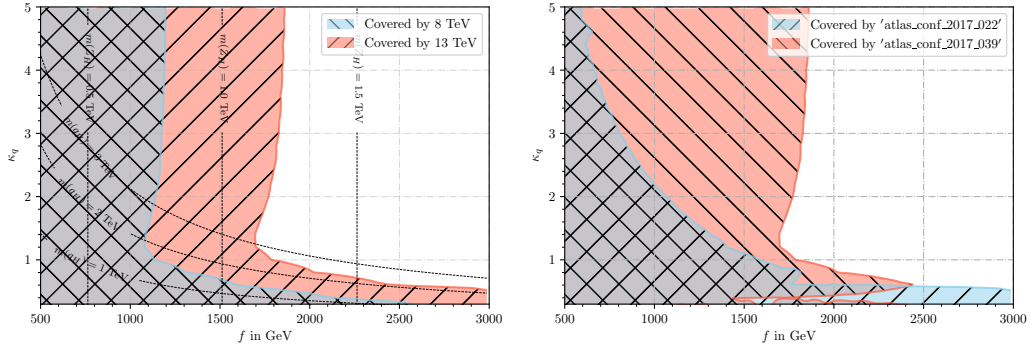


Figure 19. Results for scenario  $(Light \ell_H) \times (Heavy T^\pm) \times (TPC)$

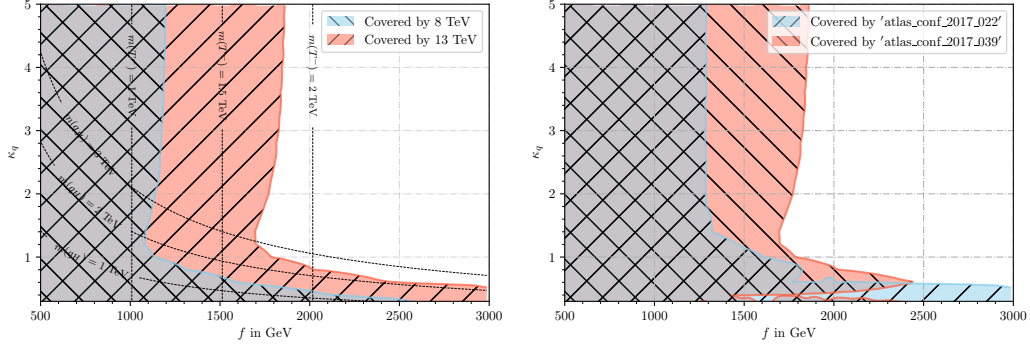


Figure 20. Results for scenario  $(Light \ell_H) \times (Light T^\pm) \times (TPC)$

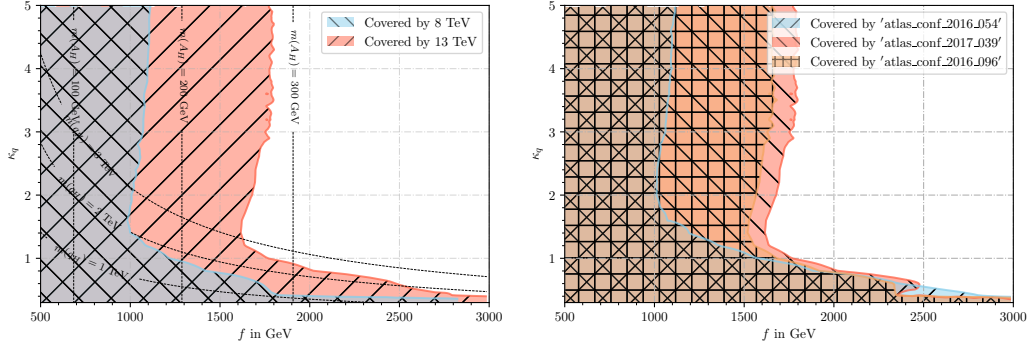


Figure 21. Results for scenario  $(Light \ell_H) \times (Heavy T^\pm) \times (TPV)$

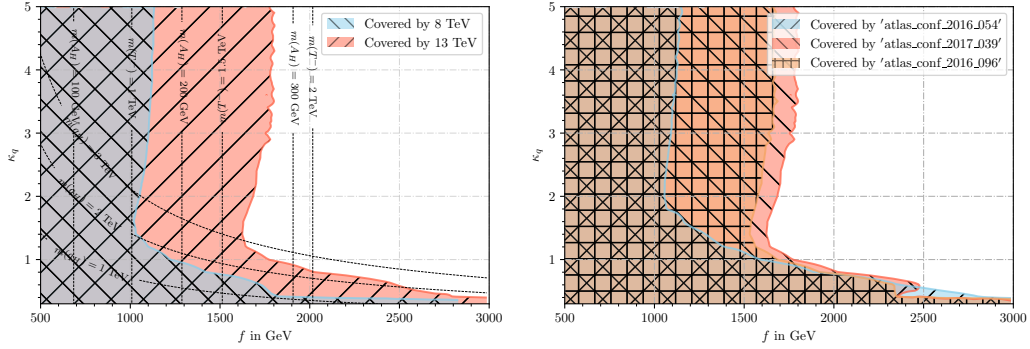


Figure 22. Results for scenario  $(Light \ell_H) \times (Light T^\pm) \times (TPV)$

### 6.3 Light $\ell_H$

In our third main benchmark scenario we again scan  $\kappa_q$  and thereby the mass of the heavy quarks. However, the degeneracy with the heavy lepton sector is now lifted by fixing  $\kappa_\ell = 0.2$ . Since we know from the results of the previous benchmark that no bound can be set if we search for the direct production of  $\ell_H$  alone, we *only* consider the effects of the light  $\ell_H$  with respect to the branching ratio of the heavy gauge bosons. Note again from our results in Sec. 5.3 that while in the *Fermion Universality* model we dominantly expect bosonic decays  $Z_H \rightarrow hA_H, W_H \rightarrow WA_H$ , the *Light Leptons* benchmark mainly produces leptonic decays  $Z_H \rightarrow \ell_H \ell, W_H \rightarrow \ell_H \nu / \nu_H \ell$  with subsequent  $\ell_H / \nu_H \rightarrow \ell / \nu A_H$ .

In Figs. 19-22 we show the results of this benchmark, again for all four subscenarios.

- As in the *Fermion Universality* scenario, we observe two main regions of exclusion which intersect at  $f \approx 1.6 \text{ TeV}$  and  $\kappa_q \approx 1.2$ .
- For small  $\kappa_q$  and large  $f$ , we again observe a  $q_H$  dominated bound similar to the one seen in the *Fermion Universality* scenario. The analysis coverage map reveals that for  $\kappa_q > 0.5$ , the bound is set by a multilepton analysis. The already mentioned  $3\ell$  signal region is very sensitive to the final state topology  $q_H q_H \rightarrow qq W_H W_H \rightarrow qq \ell \ell \ell A_H A_H$  with one of the leptons not being identified and the other three leptons being highly boosted due to the large  $q_H - W_H$  mass splitting. For  $\kappa_q < 0.5$ , the heavy vector bosons start predominantly decaying into hadronic final states — see Fig. 8 — in which case multijet final states start becoming more sensitive and reproduce the same bound as in the *Fermion Universality* scenario.
- The  $q_H$  dominated bound is again insensitive to the presence of the heavy top partners. Furthermore, it again slightly weakens in the presence of  $T$ -parity violation as the most sensitive final state stays identical but the  $\cancel{E}_T$  cut efficiency drops due to the  $A_H$  decaying.
- For larger values of  $\kappa_q$ , we again observe a nearly  $\kappa_q$ -independent absolute bound on  $f$ . This bound is again produced from direct production of heavy vector bosons and shows a small  $\kappa_q$  dependence due to the cross section dependence of this parameter, see our discussion before. Compared to the *Fermion Universality* scenario, the limit has become tremendously stronger due to the presence of light  $\ell_H$  and improves to  $f \gtrsim 1.6 \text{ TeV}$  for  $\kappa_q \approx 1.5$  and to  $f \gtrsim 2 \text{ TeV}$  for  $\kappa_q \gtrsim 5.0$ . As the analysis coverage map on the right of Fig. 19 shows, the vector-boson dominated region is now tested by the multilepton analysis which identifies the boosted leptons from the  $V_H \rightarrow \ell \ell / \nu A_H$  decays. As this final state has small Standard Model background contamination — most importantly since the leptons do not originate from  $W$  or  $Z$  decays — it produces a very clean signal and thus leads to a very strong exclusion.
- In this scenario, the presence of the heavy top partners does not improve the bound derived from heavy vector boson production at all: the bound derived from  $T^-$  production — see the *Fermion Universality* benchmark discussion — is only sensitive to scales  $f \lesssim 1350 \text{ GeV}$  and thus cannot compete with the much stronger bound set



CM identifier	Final State	Designed for	Ref.
atlas_2014_010_h1_31	$\cancel{E}_T + 3 \ell$	$\tilde{\chi}^\pm, \tilde{\chi}^0$	[59]
atlas_phys_2014_010_sq_h1	$\cancel{E}_T + 0 \ell + 2-6 j$	$\tilde{q}, \tilde{g}$	[59]
dilepton_h1	$\cancel{E}_T + 2 \ell$	$\tilde{\chi}^\pm, \tilde{\ell}$	[60]

**Table 4.** Small summary of all  $\sqrt{s} = 14$  TeV analyses which appear in the discussion of our results. More details, also on other tested analyses, are given in Tab. 5 in the appendix.

from the vector boson sector. Furthermore, the multilepton final state produced from the  $V_H$  decays do not get any contributions from any of the expected  $T^-$  decays. The limit is therefore unaffected.

- As the final state leptons from the  $V_H$  decays already produce a very clean signal, a possible decay of the  $A_H$  induced by  $T$ -parity violation only results in a smaller  $\cancel{E}_T$  cut efficiency as explained before. Thus, we only observe that the bound is slightly weakened in models with  $T$ -parity violation.

To summarize the results of this benchmark, we observe that a lighter  $\ell_H$  sector changes the decay patterns of the heavy vector bosons and this globally leads to a significant improvement on the bounds. This improvement even overcomes possible contributions from the heavy top partner sector and is only slightly weakened by the presence of  $T$ -parity violation. Therefore we again conclude that the lower limits on  $f$  derived in the *Fermion Universality* benchmark from searches for heavy vector bosons are very robust regarding changes in the heavy fermion sector.

Note that for this benchmark we chose a specific value of  $\kappa_\ell$  and thus in fact only analyzed the impact of light  $\ell_H$  for a particular assumption for their masses. It is thus worthwhile discussing how changing  $\kappa_\ell$  would affect our results:

- In our benchmark, the branching ratio  $V_H \rightarrow \ell_H \ell$  was nearly 100%. Clearly, the partial decay width  $V_H \rightarrow \ell_H \ell$  depends on the  $\ell_H$  mass and thus the leptonic branching ratio may drop if we increase the heavy lepton mass. The resulting bounds would then gradually shift from those derived in the *Light  $\ell_H$*  to those in the *Fermion Universality* benchmark.
- The kinematic configuration of the  $V_H \rightarrow \ell \ell^{(\prime)} A_H$  decay depends on the mass of the intermediate on-shell  $\ell_H$ . Changing the mass results in different expected energy distributions for the signal leptons and can therefore affect the signal acceptance after applying the cuts in analysis `atlas_conf_2017_039`. However, as the mass splitting  $V_H - A_H$  is of order 750 GeV for  $f \approx 1.5$  TeV and is independent of the benchmark model, the final state leptons are always expected to be high-energetic enough to pass the constraints.

#### 6.4 Prospects for $\sqrt{s} = 14$ TeV

As we observed in our results, the update from a center-of-mass energy of  $\sqrt{s} = 8$  TeV to  $\sqrt{s} = 13$  TeV and the increase of integrated luminosity between LHC Run 1 and Run 2

yielded significantly stronger bounds for all of the considered benchmark scenarios. In that context, the interesting question arises to which extent the sensitivity is expected to further improve at a high luminosity LHC running at  $\sqrt{s} = 14 \text{ TeV}$ . For that purpose, we used the ATLAS high luminosity studies implemented in **CheckMATE** to determine the expected bounds at very high statistics,  $\int \mathcal{L} = 3000 \text{ fb}^{-1}$ . This gives a rough estimate for the overall sensitivity range of the Large Hadron Collider to the Littlest Higgs Model in general. The corresponding cross sections are shown in Figs. 31,32 in the appendix A.

Again, all analyses which have been used by this study are listed in Tab. 5 in the appendix and we provide a shortened version in Tab. 4 which only lists those analyses which appear in our discussion of the most sensitive analyses. As one can see in the full table in Tab. 5, at this stage the list of high luminosity analyses is very limited as only few official, experimental and some phenomenological high performance studies have been implemented so far. These cover the most important topologies, i.e. missing transverse momentum with either a monojet, multijet or multileptons final state, however these old experimental studies use far fewer, less optimized signal regions compared to their counterparts at lower center-of-mass energies. Hence, our results should only be understood as rough approximations and much more sophisticated studies, especially on the experimental side, would be required to get results which are qualitatively at the same level as our earlier, detailed re-interpretation of existing experimental data.

Since the number of tested topologies is fairly small and is not expected to cover all the various final states we discussed before, we do not consider the full set of benchmark models introduced previously at this stage. Instead, we concentrate on the results for  $TPC \times \text{Heavy } T^\pm$  for the three scenarios *Fermion Universality*, *Heavy  $q_H$*  and *Light  $\ell_H$* . These give a good overview to the general expected sensitivity at high statistics. As can be seen from the results discussed above, the macroscopic structure of the excluded parameter areas are very similar for cases with and without  $T$ -parity violation and with the heavy top partners included or not. Hence, one can apply the phenomenological discussions of the previous sections to approximately determine the excluded areas for the other benchmark cases which we do not explicitly discuss in the following.

The results of our scans are shown in Figs. 23-25. Note the extended  $f$ -axis range compared to Figs. 11-22 to better illustrate the even higher  $f$ -reach at high center-of-mass energies. The figures on the left column again show the overall expected experimental reach at 14 TeV and compare to current results from 13 TeV data which corresponds to the results discussed in the previous sections. The figures in the right column, similarly to before, show the most sensitive analyses in different regions of parameter space. Fluctuations in the contours originate from sizable statistical uncertainties in our Monte Carlo description<sup>9</sup>, however do not affect the qualitative description of the overall bound.

In general, the structure of the bounds is kept, i.e. there is a (nearly)  $\kappa$ -independent bound for small  $f$  and larger values of  $\kappa$  while there is a bound which follows the iso-mass contours for large values of  $f$ .

---

<sup>9</sup>We use the same sample size as in our previous studies, however due to the 100-fold integrated luminosity the statistical uncertainty near the boundary increases approximately by a factor of 10.

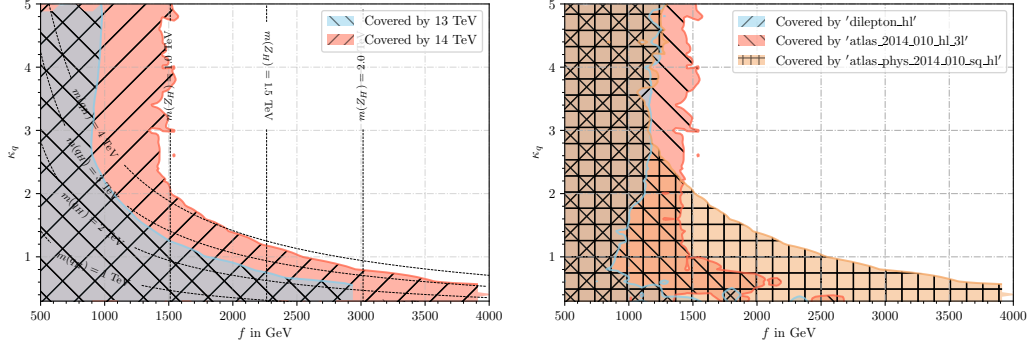


**Figure 23.** Expected results at  $\sqrt{s} = 14 \text{ TeV}$ ,  $f\mathcal{L} = 3000 \text{ fb}^{-1}$  for scenario  $(\text{Fermion Universality}) \times (\text{Heavy } T^\pm) \times (\text{TPC})$ .

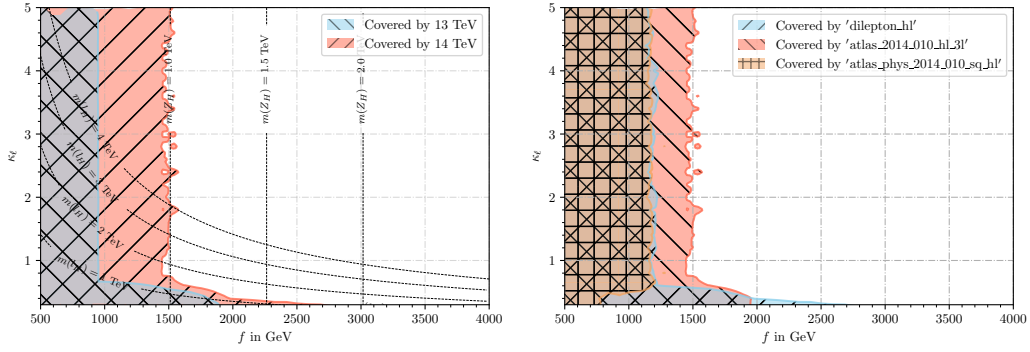


**Figure 24.** Expected results at  $\sqrt{s} = 14 \text{ TeV}$ ,  $f\mathcal{L} = 3000 \text{ fb}^{-1}$  for scenario  $(\text{Heavy } q_H) \times (\text{Heavy } T^\pm) \times (\text{TPC})$ .

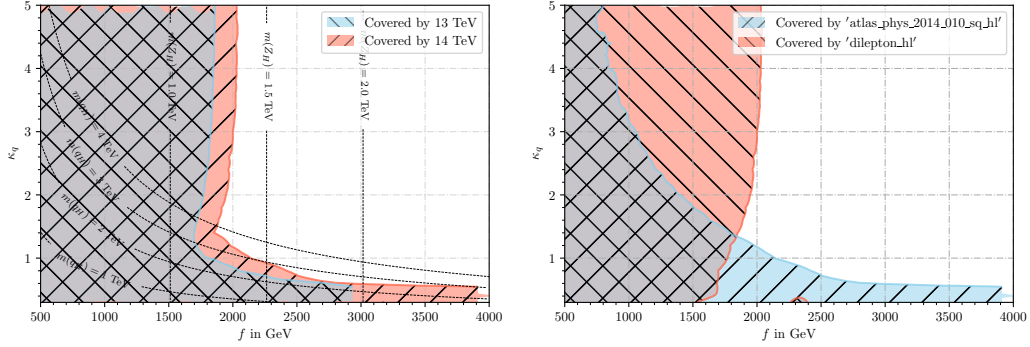


**Figure 25.** Expected results at  $\sqrt{s} = 14 \text{ TeV}$ ,  $f\mathcal{L} = 3000 \text{ fb}^{-1}$  for scenario  $(\text{Light } \ell_H) \times (\text{Heavy } T^\pm) \times (\text{TPC})$ .

- In the *Fermion Universality* scenario, the  $q_H$  mass bound for large values of  $f$  increases by 1 to 1.5 TeV and excludes heavy quarks with masses  $m(q_H) \gtrsim 4 \text{ TeV}$  for  $f \approx 2 \text{ TeV}$  and  $m(q_H) \gtrsim 3 \text{ TeV}$  for  $f \approx 4 \text{ TeV}$ . As before, this bound originates from the high luminosity version of a multijet plus  $\cancel{E}_T$  search designed to find heavy squarks or gluinos in supersymmetry. The  $V_H$  dominated bound for large values of  $\kappa$  probes heavy vector boson masses of order 1 TeV. Compared to the previous result determined

at 13 TeV, the most sensitive analysis is now quoted to be the multilepton instead of the multijet final state. To reduce the contamination from pileup which is expected to become an important issue for the high luminosity LHC, the multijet final states require the scalar sum of the transverse momenta of all reconstructed objects to exceed 3 TeV. In the  $V_H$  dominated region, the expected signal  $V_H \rightarrow A_H V, V \rightarrow$  hadrons with  $m(V_H) \approx 1$  TeV typically does not pass this constraint and for example requires a boosted final state due to a high  $p_T$  jet from initial-state radiation (ISR) whose requirement significantly reduces the expected event rate.

- The *Heavy*  $q_H$  scenario at  $\sqrt{s} = 14$  TeV does not significantly improve the  $\ell_H$ -induced bound for small values of  $\kappa$ . We expect a weak bound which follows the  $\ell_H$  mass contour and excludes masses of order  $m(\ell_H) \approx 1 - 1.5$  TeV. This bound originates from an extrapolated search for dilepton final states. This is however only a minor improvement to the bound which can be set already from today's result. As in the previous benchmark scenario, the  $V_H$  produces a  $\kappa$ -independent bound of  $m(V_H) \gtrsim 1$  TeV.
- Lastly, the bound in the *Light*  $\ell_H$  scenario only improves little compared to the current 13 TeV results. In the large  $f$  region, the most sensitive analysis channel at LHC Run 2 is a multijet final state with one additional lepton which has a particularly small Standard Model contamination. Unfortunately, we do not have a high luminosity version of this analysis available and can only consider final states with many jets but no final state lepton. As the characteristic feature of the the *Light*  $\ell_H$  scenario is the appearance of at least one lepton in all relevant final state decay chains, we lose sensitivity due to our restricted amount of available analyses. For larger values of  $\kappa$ , the bound on  $m(V_H)$  only increases by about 100 GeV, determined from a search which requires two leptons in the final state. This analysis is designed to target either of the two supersymmetric topologies  $\tilde{\ell}\tilde{\ell} \rightarrow \ell\ell\tilde{\chi}\tilde{\chi}$  or  $\tilde{\chi}^+\tilde{\chi}^- \rightarrow WW\tilde{\chi}\chi$  followed by leptonic  $W$  decays. Though some of the final states produced by our benchmark scenario pass the constraints set for these particular topologies, none of the signal regions are specifically designed for our topology. Thus, again our bound does not represent the full sensitivity which can be expected from the high luminosity LHC but significant additional effort would be required to determine the necessary experimental predictions for our desired topologies.

## 7 Comparison of LHC limits with Bounds from Electroweak Precision Observables

In the previous section we discussed the bounds which can be put on various benchmark scenarios of the Littlest Higgs Model with  $T$ -parity (and its possible violation). As explained in Sec. 2, an appealing property of this model is its considerably small amount of fine tuning in the Higgs sector. Moreover, not only do the null results of searches for these new  $T$ -odd particles set bounds on this model but also, see Sec. 3, electroweak precision observables (EWPO) put tight constraints on  $f$  and  $\kappa$ . In the following we want to combine these three

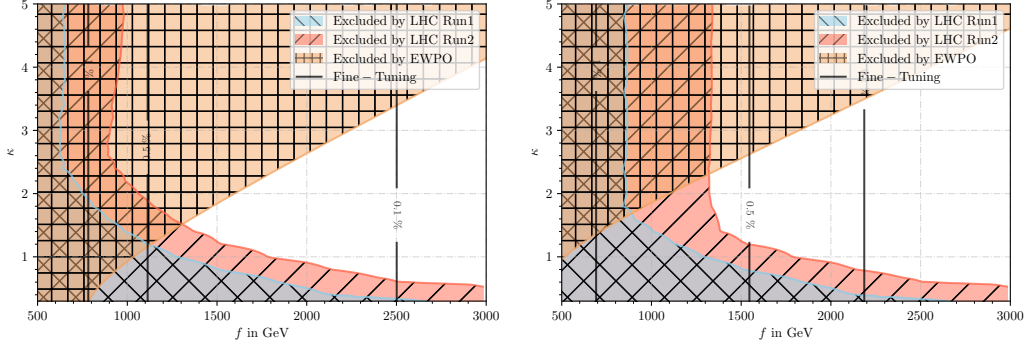


**Figure 26.** Combined results for scenario  $(Fermion\ Universality) \times (TPC)$ , left:  $Heavy\ T^\pm$ , right:  $\times(Light\ T^\pm)$

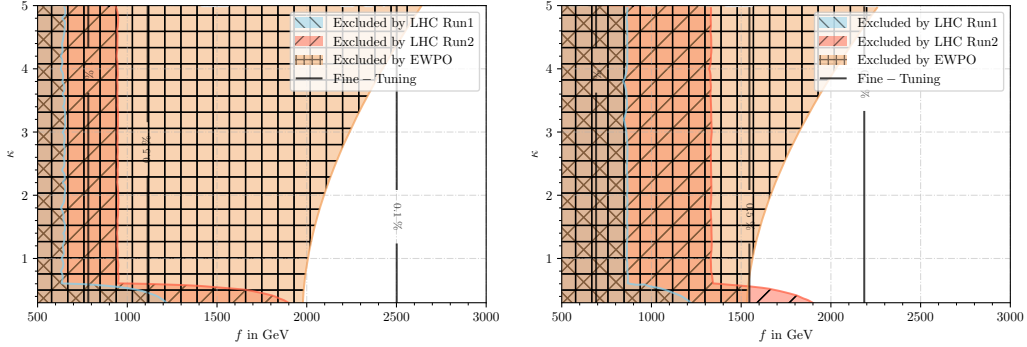


**Figure 27.** Combined results for scenario  $(Heavy\ q_H) \times (TPC)$ , left:  $Heavy\ T^\pm$ , right:  $\times(Light\ T^\pm)$

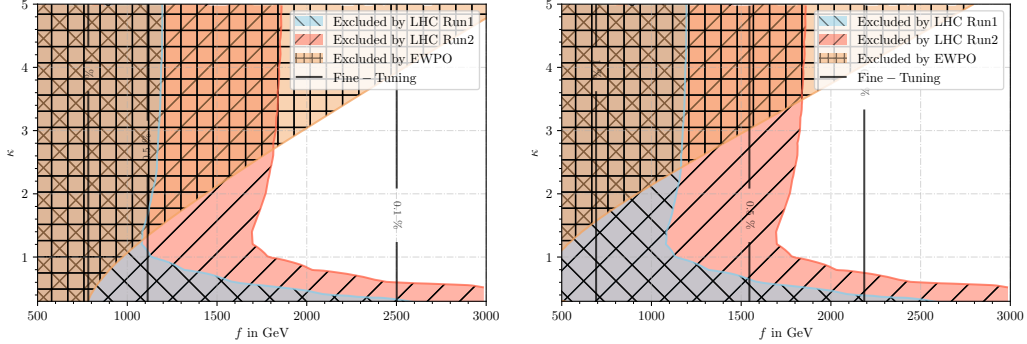


**Figure 28.** Combined results for scenario  $(Light\ \ell_H) \times (TPC)$ , left:  $Heavy\ T^\pm$ , right:  $\times(Light\ T^\pm)$

pieces of information, putting a particular focus on the relevance of the newest LHC results for the total combined bound on the model.

In Figs. 26-28 we show compilations of bounds from electroweak precision observables, see Sec. 3, the amount of fine tuning in the Higgs sector according to Eq. (2.27) and the 8 and 13 TeV LHC bounds discussed in Sec. 6. We only show results for the case of  $T$ -parity conservation as electroweak precision observables are not affected by the presence of  $T$ -parity violating operators and the respective TPV collider bounds are very similar, see our results of the previous section. In each figure we show the results for  $Heavy\ T^\pm$  scenario,

i.e.  $R = 0.2$ , and *Light*  $T^\pm$  scenario, i.e.  $R = 1.0$ . Note that the choice of this parameter has an important impact on the fine tuning measure  $\Delta$ .

In general, we observe that LHC results produce an absolute lower bound on  $f$  for large  $\kappa$  and a lower bound which approximately follows  $f \cdot \kappa$  for small  $\kappa$ . Electroweak precision data, however, tend to produce upper bounds which approximately follow the ratio  $f/\kappa$ . Therefore, we have two very complementary bounds which together exclude a considerably large region of parameter space. This complementarity mostly originates from the opposite dependence of the respective bounds on  $\kappa$  and  $R$ : the collider data produce stronger bounds for lighter particles and therefore show their largest sensitivity for small values of  $\kappa$  and/or  $R = 1.0$ . Loop corrections to precision observables, however, increase if the corresponding coupling constants increase and therefore show their strictest bounds for *large* values of  $\kappa$  and  $R = 0.2$ .<sup>10</sup>

We now move the general discussion to some individual results of particular benchmark models:

- In the case of *Lepton Universality*, we observe that the updated collider results from 13 TeV are only relevant in the regions dominated by  $q_H$  and  $T^\pm$  production. Most importantly, bounds derived from  $V_H V_H$  production only cover the region  $f < 1 \text{ TeV}, \kappa > 2$  and are not competitive with the limits from electroweak precision data which cover the same region in the *Light*  $T^\pm$  scenario and an even much larger region  $f < 1.3 \text{ TeV}, \kappa > 1.5$  in the case of *Heavy*  $T^\pm$ .

In the case of *Heavy*  $T^\pm$ , the combined bound from electroweak precision observables and  $q_H$  production excludes symmetry breaking scales  $f$  below 1.3 TeV, independent of  $\kappa$ , and by that requires a fine tuning below 0.5%. If the heavy top partners  $T^\pm$  are lighter, the EWPO bounds weaken. However, at the same time the collider bounds increase, resulting in approximately the same bound of  $f > 1.3 \text{ TeV}$  as before which however corresponds to a slightly smaller fine tuning of approximately 0.6%. Judging from the two benchmark scenarios for  $T^\pm$ , we conclude that the combination of electroweak precision data and newest LHC results does not allow for values of  $f < 1.3 \text{ TeV}$  for values of  $R \in [0.2, 1.0]$ . As the EWPO bounds become stronger for heavier  $T^\pm$  and the collider result becomes stricter for lighter  $T^\pm$ , the lower bound on  $f$  should become even stricter for any value of  $R$  outside this range.

- The combined results of the *Heavy*  $q_H$  scenario show a similar complementarity effect as in the previous model: whilst the LHC results are significantly weakened if the heavy quarks are decoupled, the bounds from electroweak precision observables become even stricter due to their dependence on  $\kappa^2$ , see Sec. 3, and thus become stronger if  $\kappa_q = 3.0$  is fixed. Here, the bounds implicitly depend on the value of  $R$  and exclude values of  $f$  below 1.5 TeV for  $R = 1.0$  (*Light*  $T^\pm$ ), and values below 2 TeV for  $R = 0.2$  (*Heavy*  $T^\pm$ ). Even in the case of *Light*  $T^\pm$  the LHC result cannot compete. Still, the bounds are already very close to the EWPO limit such that we

---

<sup>10</sup>Note that the free parameter  $R$  defines the Yukawa coupling  $\lambda_2$  via Eq. (2.14) which *increases* if  $R$  *decreases*.

again conclude that any other value of  $R$  should not produce a significantly weaker but potentially an even stronger bound on  $f$  if the mass of the  $T^\pm$  is chosen even lighter. Note that for very small values of  $\kappa_\ell$ , the LHC bound derived from  $V_H \rightarrow \ell_H \ell$  pushes the lower bound on  $f$  by a few hundred GeV, but not considerably. The minimal allowed fine tuning is around 0.5% for the *Light*  $T^\pm$  scenario and reduces to approximately 0.25% for the *Heavy*  $T^\pm$  scenario.

- For the *Light*  $\ell_H$  scenario, the complementarity between LHC and EWPO results appears in the opposite direction as before: Due to the small value of  $\kappa_\ell$ , electroweak precision observables are slightly weaker than in the previous benchmark cases. However, at the same time the collider bounds improve significantly due to the very distinctive decay topology which produces several hard leptons, see our discussion in the previous section. In this benchmark, the lower bound  $f > 1.7$  TeV originates solely from the collider result and is independent of the details of the heavy top partner sector. It is only the region with large values of  $f \gtrsim 1.8$  TeV,  $\kappa \gtrsim 2.5$  where the EWPO bound may become more relevant — depending on the chosen value of  $R$ . The minimal allowed fine tuning is around 0.35% in the *Heavy*  $T^\pm$  and 0.4% in the *Light*  $T^\pm$  scenario, respectively.

All in all, we observe that without taking the LHC data into account, fine tuning above 1% would still be allowed in regions with light  $q_H$  and light  $T^\pm$ . These regions, however, are nowadays testable at collider experiments and results from the first LHC run at 8 TeV already pushed the fine-tuning to the sub-percent level. Using the updated results acquired during the  $\sqrt{s} = 13$  TeV period, limits derived from the Large Hadron Collider become more and more severe. Though the precise position of the total bound depends on the details of the heavy fermion sector, the heavy top partner masses, and the presence or absence of  $T$ -parity violation, we observe that due to their complementary behavior regarding the EWPO bounds, values of  $f$  below 1.3 TeV and fine-tuning above 0.6% seems to be excluded by now. Within our considered benchmark scenarios we observe that *Fermion Universality* is the most weakly constrained model. However, the newest 13 TeV results show a significant improvement already when put in comparison with the earlier 8 TeV bounds. Furthermore, our approximate future sensitivity study in Sec. 6.4 gives us reason to expect an even further improvement by LHC results in the near and far future, putting the Littlest Higgs Model with  $T$  parity more and more to the test.

## 8 Summary

In this study we reinterpreted null results from LHC searches for physics beyond the Standard Model in the context of the Littlest Higgs Model with conserved and broken  $T$ -parity. This model is an elegant implementation of global collective symmetry breaking combined with a discrete symmetry to explain the natural lightness of the Higgs boson as a (pseudo-)Nambu-Goldstone boson. Bounds on the symmetry-breaking scale  $f$  from data until 2013 were still as low as roughly 600 GeV. This model predicts heavy partners for the Standard Model quarks  $q_H$ , leptons  $\ell_H$ , gauge bosons  $W_H, Z_H, A_H$  and special partners for the

top quark  $T^\pm$ . The mass hierarchies and the presence of the discrete  $T$ -parity result in a model which shares many phenomenological similarities with supersymmetric extensions of the Standard Model, most importantly it features a stable, invisible  $A_H$  if  $T$ -parity is conserved, similar to the lightest neutralino in supersymmetry with conserved  $R$ -parity.

Using the degrees of freedom for the full theory, we defined a set of benchmark scenarios which make different assumptions about the mass hierarchies in the heavy fermion sector, the masses of the heavy top partners and the possible presence of small  $T$ -parity violating operators. By making use of the collider phenomenology tool **CheckMATE**, we systematically analyzed all relevant topologies at the LHC and derived bounds for all benchmark scenarios, excluding those regions which would have predicted a signal in any of the many considered search channels. We also give rough estimates for the bounds expected from a high luminosity LHC running with  $\sqrt{s} = 14$  TeV and  $3 \text{ ab}^{-1}$  of integrated luminosity.

Our results show that  $q_H$  pair production,  $V_H$  pair production and  $T^-$  pair production, respectively, produce strong bounds in the model parameter space due to null results in searches dedicated for squarks and electroweakinos in supersymmetry. Most importantly, searches which require a large amount of hard jets and a significant amount of missing transverse momentum produce the strongest results in regions where  $q_H$  and  $T^-$  production is important whilst searches for final states with multilepton and missing energy become more relevant as soon as heavy vector boson production is the dominant channel. Color-neutral heavy leptons are mostly irrelevant for the LHC, unless they are light enough to appear in decay topologies like  $V_H \rightarrow \ell_H \ell$  in which case they are again largely constrained by searches for multileptons and missing energy. Allowing for a small amount of  $T$ -parity violation surprisingly only has a minor impact on the result if compared to the case where  $T$ -parity is exactly conserved. This can be explained by the fact that in the case of  $T$ -parity violation via anomalous WZW-terms,  $A_H$  decays predominantly into the Standard Model gauge bosons whose leptonic decays can produce the required missing energy plus additional hard particles which improve the signal-to-background ratio.

As the masses of the particles  $q_H, \ell_H, V_H$  and  $T^\pm$  depend differently on the Yukawa-like parameters  $\kappa_q, \kappa_\ell$  and  $R$ , precise LHC bounds depend on the particular values of these three parameters. On the other hand, all particle masses grow linearly with the symmetry breaking scale  $f$  and we conclude that LHC results from the  $\sqrt{s} = 13$  TeV run exclude any value of  $f$  below 950 GeV at 95% confidence level. The weakest bound appears in a scenario where only the heavy gauge bosons are kinematically accessible and all Yukawa parameters are such that the other particles are decoupled from LHC observability.

Our LHC bounds are complementary to those derived from electroweak precision observables as the former constrain light particles with small Yukawa couplings while the latter put limits on sizable contributions from large Yukawa couplings. This complementarity strongly removes the dependence of the bound on the details of the heavy fermion sector as weaker limits from the LHC are compensated by corresponding stronger bounds from EWPO and vice versa. All in all, from our benchmark results we conclude that the symmetry breaking scale  $f$  must be larger than 1.3 TeV and the fine tuning cannot be better than 0.4%. Even stronger bounds are possible if more details about the heavy fermion sector are known and these limits can easily be derived from our exhaustive set of results



for the various benchmark scenarios. This constitutes an improvement of more than 700 GeV compared to LHC run 1 data.

Though the Littlest Higgs model with  $T$ -parity has been constrained much stronger by LHC run 2 data, it is still a rather natural solution to the shortcomings of the electroweak and scalar sector, and we will need full high-luminosity data from the LHC to decide whether naturalness is actually an issue of the electroweak sector or not. A qualitative improvement of all bounds on the model, particularly in the Higgs sector and the heavy lepton sector, might need the running of a high-energy lepton collider (or a hadron collider at much higher energy).

## Acknowledgments

The authors like to thank Marco Tonini for helping in the validation of our results. SYS would like to thank Pedro Schwaller for clarifications regarding the  $T$ -parity violating decays. JRR likes to thank Maxim Perelstein for helpful discussions. DD and JRR acknowledge funding and support from the Collaborative Research Unit (SFB) 676 of the Deutsche Forschungsgemeinschaft (DFG), projects B1 and B11.

## A Supplementary Figures for the Collider Analysis

In this section we provide additional figures which are useful to better understand and/or reproduce our results but which are not necessarily needed for the discussion of the main text.

This includes the cross sections for a center-of-mass energy of 8 TeV in Fig. 29 for the *Fermion Universality/Light  $\ell_H + Light T^\pm$*  scenario as a function of the Little Higgs scale  $f$  and  $\kappa_q$ , respectively. In Fig. 30 we show the 8 TeV cross sections for the *Heavy  $q_H + Light T^\pm$*  scenario. The lower figures, Fig. 31 and Fig. 32, show the cross sections for the same scenarios, but now for 14 TeV full LHC center-of-mass energies.

## B Full List of CheckMATE Analyses

Table 5 gives the full list of used CheckMATE analyses. The first column shows the CheckMATE identifier, the second the purpose for which the analysis was designed for. The last three columns show the number of signal regions in the corresponding analysis (marked #SR), the integrated luminosity for that analysis and the reference to the publication or conference notes from the experimental collaborations. More details on the respective analyses and corresponding validation material can be found on <http://checkmate.hepforge.org>. High luminosity analyses marked with \* do not correspond to official experimental studies but have been implemented by the CheckMATE collaboration. More information can be found in the respective references.

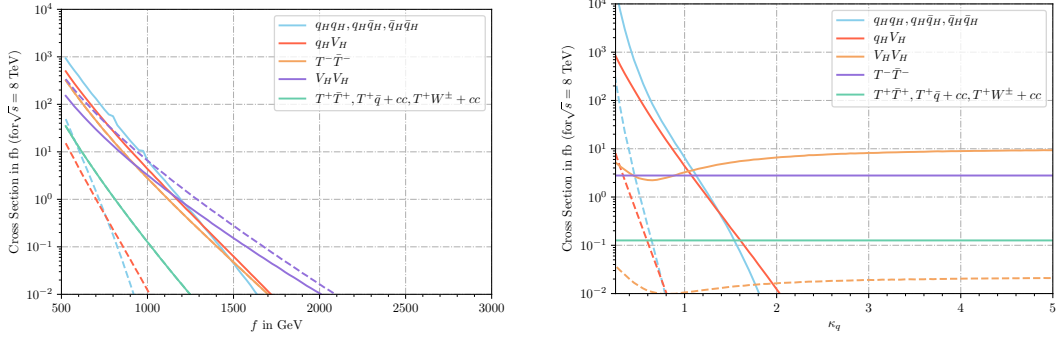


Figure 29. Same as Fig. 1 for  $\sqrt{s} = 8$  TeV.

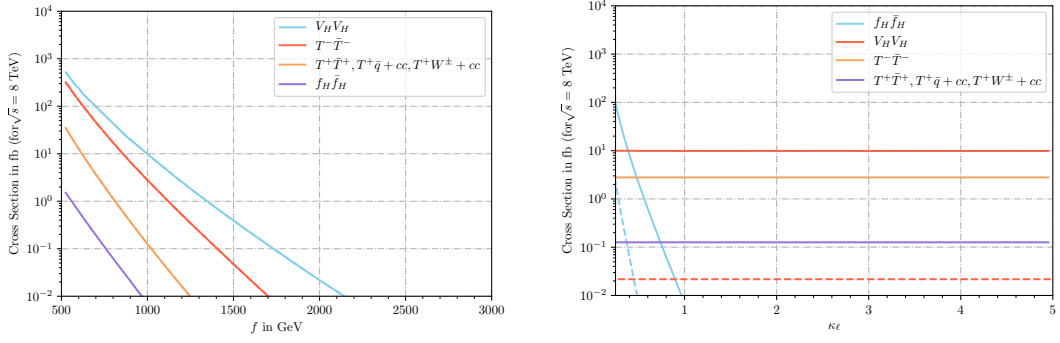


Figure 30. Same as Fig. 29 for benchmark model *Heavy*  $q_H$  + *Light*  $T^\pm$ .

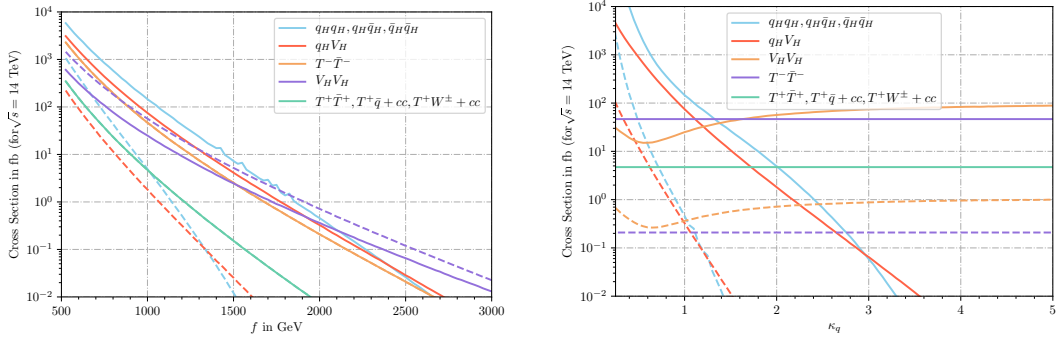


Figure 31. Same as Fig. 1 for  $\sqrt{s} = 14$  TeV.

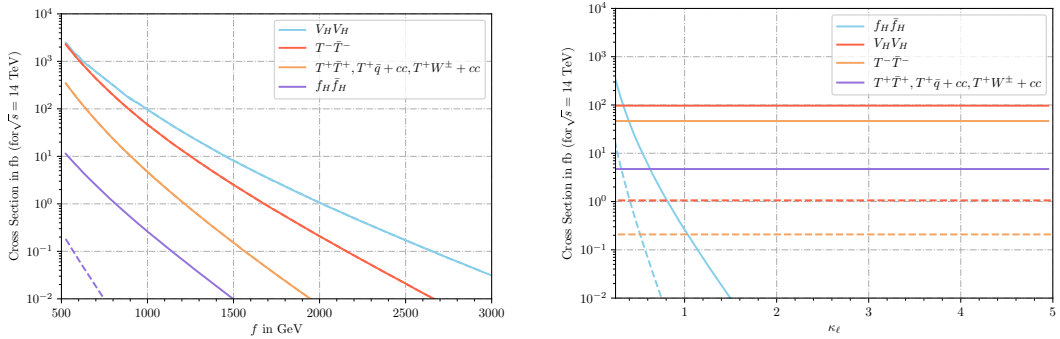


Figure 32. Same as Fig. 31 for benchmark model *Heavy*  $q_H$  + *Light*  $T^\pm$ .

CheckMATE identifier	Search designed for	#SR	$L_{\text{int}}$	Ref.
$\sqrt{s} = 8 \text{ TeV}$				
atlas_1308_1841	New phenomena in final states with large jet multiplicities and $\cancel{E}_T$	13	20.3	[61]
atlas_1308_2631	Direct $\tilde{t}/\tilde{b}$ pair production in final states with $\cancel{E}_T$ and two $b$ -jets	6	20.1	[62]
atlas_1402_7029	Direct production of $\tilde{\chi}^\pm/\tilde{\chi}^0$ in events with 3 $\ell$ and $\cancel{E}_T$	20	20.3	[63]
atlas_1403_4853	Direct $\tilde{t}$ pair production in final states with $2\ell$	12	20.3	[64]
atlas_1403_5222	Direct $t$ pair production in events with a $Z$ , $b$ -jets and $\cancel{E}_T$	5	20.3	[65]
atlas_1404_2500	Supersymmetry in final states with jets and 2 SS $\ell$ or $3\ell$	5	20.3	[66]
atlas_1405_7875	Search for $\tilde{q}$ and $\tilde{g}$ in final states with jets and $\cancel{E}_T$	15	20.3	[67]
atlas_1407_0583	$\tilde{t}$ pair production in final states with 1 isol. $\ell$ , jets and $\cancel{E}_T$	27	20.3	[68]
atlas_1407_0608	Pair produced 3rd gen. squarks decaying via $c$ or compressed scenarios	3	20.3	[69]
atlas_1411_1559	New phenomena in events with a photon and $\cancel{E}_T$	1	20.3	[70]
atlas_1501_07110	Direct production of $\tilde{\chi}^\pm/\tilde{\chi}^0$ decaying into a Higgs boson	12	20.3	[71]
atlas_1502_01518	New phenena in final states with an energetic jet and large $\cancel{E}_T$	9	20.3	[53]
atlas_1503_03290	Supersymmetry in events with an SFOS $\ell$ pair, jets and large $\cancel{E}_T$	1	20.3	[72]
atlas_1506_08616	Direct Pair production third generation squarks	12	20.0	[73]
atlas_conf_2012_104	Supersymmetry in final states with jets, 1 isolated lepton and $\cancel{E}_T$	2	5.8	[74]
atlas_conf_2013_024	Direct $\tilde{t}$ pair production in the all-hadronic $t\bar{t} + \cancel{E}_T$ final state	3	20.5	[75]
atlas_conf_2013_049	Direct $\tilde{\ell}/\tilde{\chi}^\pm$ production in final states with 2 OS $\ell$ , no jets and $\cancel{E}_T$	9	20.3	[76]
atlas_conf_2013_061	Strongly produced Supersymmetric particles with $\geq 3$ $b$ -jets and $\cancel{E}_T$	9	20.1	[77]
atlas_conf_2013_089	Strongly produced Supersymmetric particles decaying into 2 leptons	12	20.3	[78]
atlas_conf_2015_004	Invisibly decaying Higgs bosons produced in vector boson fusion	1	20.3	[79]
atlas_conf_2012_147	New phenomena in monojets plus $\cancel{E}_T$	4	10.0	[80]
atlas_conf_2013_035	Direct production of $\tilde{\chi}^\pm/\tilde{\chi}^0$ in events with 3 leptons and $\cancel{E}_T$	6	20.7	[81]
atlas_conf_2013_037	Direct $t$ pair production in final states with 1 isolated $\ell$ , jets and $\cancel{E}_T$	6	20.7	[82]
atlas_conf_2013_047	$\tilde{q}$ and $\tilde{g}$ in final states with jets and $\cancel{E}_T$	10	20.3	[83]
cms_1303_2985	Supersymmetry in hadronic final states with $b$ -jets and $\cancel{E}_T$ using $\alpha_T$	59	11.7	[84]
cms_1408_3583	Dark Matter, Extra Dimensions and Unparticles in monojet events	7	19.7	[85]
cms_1502_06031	New Physics in events with $2\ell$ , jets and $\cancel{E}_T$	6	19.4	[86]
cms_1504_03198	Dark Matter produced in association with $t\bar{t}$ in final states with $1\ell$	1	19.7	[87]
cms_sus_13_016	Supersymmetry in events with 2 OS $\ell$ , many jets, $b$ -jets and large $\cancel{E}_T$	1	19.5	[88]
cms_exo_14_014	Heavy Majorana neutrinos in events with SS dileptons and jets	16	19.7	[89]
$\sqrt{s} = 13 \text{ TeV}$				
atlas_1602_09058	Supersymmetry in final states with jets and two SS leptons or 3 leptons	4	3.2	[90]
atlas_1604_01306	New phenomena in events with a photon and $\cancel{E}_T$	1	3.2	[91]
atlas_1604_07773	New phenomena in final states with an energetic jet and large $\cancel{E}_T$	13	3.2	[92]
atlas_1605_03814	$\tilde{q}$ and $\tilde{g}$ in final states with jets and $\cancel{E}_T$	7	3.2	[93]
atlas_1605_04285	Gluginos in events with an isolated lepton, jets and $\cancel{E}_T$	7	3.3	[94]
atlas_1605_09318	Pair production of $\tilde{g}$ decaying via $\tilde{t}$ or $\tilde{b}$ in events with $b$ -jets and $\cancel{E}_T$	8	3.3	[95]
atlas_1606_03903	$\tilde{t}$ in final states with one isolated lepton, jets and $\cancel{E}_T$	3	3.2	[96]
atlas_1609_01599	Measurement of $t\bar{t}V$ cross sections in multilepton final states	9	3.2	[97]
atlas_conf_2015_082	Supersymmetry in events with leptonically decaying $Z$ , jets and $\cancel{E}_T$	1	3.2	[98]
atlas_conf_2016_013	Vector-like $t$ pairs or 4 $t$ in final states with leptons and jets	10	3.2	[99]
atlas_conf_2016_050	$\tilde{t}$ in final states with one isolated lepton, jets and $\cancel{E}_T$	5	13.3	[100]
atlas_conf_2016_054	$\tilde{q}$ , $\tilde{g}$ in events with an isolated lepton, jets and $\cancel{E}_T$	10	14.8	[56]
atlas_conf_2016_076	Direct $\tilde{t}$ pair production and DM production in final states with $2\ell$	6	13.3	[101]
atlas_conf_2016_078	Further searches for $\tilde{q}$ and $\tilde{g}$ in final states with jets and $\cancel{E}_T$	13	13.3	[102]
atlas_conf_2016_096	Supersymmetry in events with $2\ell$ or $3\ell$ and $\cancel{E}_T$	8	13.3	[55]
atlas_conf_2017_022	$\tilde{q}$ , $\tilde{g}$ in final states with jets and $\cancel{E}_T$	24	36.1	[57]
atlas_conf_2017_039	Electroweakino production in final states with 2 or 3 leptons	37	36.1	[58]
atlas_conf_2017_040	Dark Matter or invisibly decaying $h$ , produced in associated with a $Z$	2	36.1	[103]
cms_pas_sus_15_011	New physics in final states with an OSSF lepton pair, jets and $\cancel{E}_T$	47	2.2	[104]
$\sqrt{s} = 14 \text{ TeV}$				
atlas_phys_pub_2013_011	Search for Supersymmetry at the high luminosity LHC ( $\tilde{t}$ sector)	4	3000	[105]
atlas_2014_010_hl_31	Search for Supersymmetry at the high luminosity LHC ( $\tilde{\chi}^\pm/\tilde{\chi}^0$ sector)	1	3000	[59]
atlas_phys_2014_010_sq_hl	Search for Supersymmetry at the high luminosity LHC ( $\tilde{q}/\tilde{g}$ sector)	10	3000	[59]
dilepton_hl*	Custom Search for $\tilde{\ell}/\tilde{\chi}^\pm$ in final states with 2 leptons and $\cancel{E}_T$	9	3000	[60]
atlas_14tev_monojet*	Custom Search for DM in final states with an energetic jet and $\cancel{E}_T$	5	3000	[106]

**Table 5.** Full list of all CheckMATE analyses used for this study. The column labelled #SR yields the number of signal regions. Entries for the integrated luminosities  $L_{\text{int}}$  are given in  $\text{fb}^{-1}$ .

## References

- [1] ATLAS Collaboration, G. Aad et al., *Observation of a new particle in the search for the*

- Standard Model Higgs boson with the ATLAS detector at the LHC*, *Phys. Lett.* **B716** (2012) 1–29, [[arXiv:1207.7214](#)].
- [2] CMS Collaboration, S. Chatrchyan et al., *Observation of a new boson at a mass of 125 GeV with the CMS experiment at the LHC*, *Phys. Lett.* **B716** (2012) 30–61, [[arXiv:1207.7235](#)].
- [3] N. Arkani-Hamed, A. G. Cohen, and H. Georgi, *Electroweak symmetry breaking from dimensional deconstruction*, *Phys. Lett.* **B513** (2001) 232–240, [[hep-ph/0105239](#)].
- [4] N. Arkani-Hamed, A. G. Cohen, T. Gregoire, and J. G. Wacker, *Phenomenology of electroweak symmetry breaking from theory space*, *JHEP* **08** (2002) 020, [[hep-ph/0202089](#)].
- [5] H. Georgi and A. Pais, *Vacuum Symmetry and the PseudoGoldstone Phenomenon*, *Phys. Rev.* **D12** (1975) 508.
- [6] D. B. Kaplan and H. Georgi,  *$SU(2) \times U(1)$  Breaking by Vacuum Misalignment*, *Phys. Lett.* **136B** (1984) 183–186.
- [7] D. E. Kaplan, M. Schmaltz, and W. Skiba, *Little Higgses and turtles*, *Phys. Rev.* **D70** (2004) 075009, [[hep-ph/0405257](#)].
- [8] N. Arkani-Hamed, A. G. Cohen, E. Katz, and A. E. Nelson, *The Littlest Higgs*, *JHEP* **07** (2002) 034, [[hep-ph/0206021](#)].
- [9] W. Kilian, D. Rainwater, and J. Reuter, *Pseudo-axions in little Higgs models*, *Phys. Rev.* **D71** (2005) 015008, [[hep-ph/0411213](#)].
- [10] M. Perelstein, *Little Higgs models and their phenomenology*, *Prog. Part. Nucl. Phys.* **58** (2007) 247–291, [[hep-ph/0512128](#)].
- [11] W. Kilian, D. Rainwater, and J. Reuter, *Distinguishing little-Higgs product and simple group models at the LHC and ILC*, *Phys. Rev.* **D74** (2006) 095003, [[hep-ph/0609119](#)]. [Erratum: *Phys. Rev.* **D74**, 099905 (2006)].
- [12] H.-C. Cheng and I. Low, *TeV symmetry and the little hierarchy problem*, *JHEP* **09** (2003) 051, [[hep-ph/0308199](#)].
- [13] H.-C. Cheng and I. Low, *Little hierarchy, little Higgses, and a little symmetry*, *JHEP* **08** (2004) 061, [[hep-ph/0405243](#)].
- [14] C. T. Hill and R. J. Hill,  *$T^-$  parity violation by anomalies*, *Phys. Rev.* **D76** (2007) 115014, [[arXiv:0705.0697](#)].
- [15] C. T. Hill and R. J. Hill, *Topological Physics of Little Higgs Bosons*, *Phys. Rev.* **D75** (2007) 115009, [[hep-ph/0701044](#)].
- [16] J. Hubisz and P. Meade, *Phenomenology of the littlest Higgs with  $T$ -parity*, *Phys. Rev.* **D71** (2005) 035016, [[hep-ph/0411264](#)].
- [17] L. Wang, J. M. Yang, and J. Zhu, *Dark matter in the little Higgs model under current experimental constraints from the LHC, Planck, and Xenon data*, *Phys. Rev.* **D88** (2013), no. 7 075018, [[arXiv:1307.7780](#)].
- [18] A. Freitas, P. Schwaller, and D. Wyler, *Consequences of  $T$ -parity breaking in the Littlest Higgs model*, *JHEP* **09** (2008) 013, [[arXiv:0806.3674](#)].
- [19] J. Reuter, M. Tonini, and M. de Vries, *Littlest Higgs with  $T$ -parity: Status and Prospects*, *JHEP* **02** (2014) 053, [[arXiv:1310.2918](#)].

- [20] C. Csaki, J. Hubisz, G. D. Kribs, P. Meade, and J. Terning, *Big corrections from a little Higgs*, *Phys. Rev.* **D67** (2003) 115002, [[hep-ph/0211124](#)].
- [21] J. L. Hewett, F. J. Petriello, and T. G. Rizzo, *Constraining the littlest Higgs*, *JHEP* **10** (2003) 062, [[hep-ph/0211218](#)].
- [22] T. Han, H. E. Logan, B. McElrath, and L.-T. Wang, *Phenomenology of the little Higgs model*, *Phys. Rev.* **D67** (2003) 095004, [[hep-ph/0301040](#)].
- [23] W. Kilian and J. Reuter, *The Low-energy structure of little Higgs models*, *Phys. Rev.* **D70** (2004) 015004, [[hep-ph/0311095](#)].
- [24] M. Blanke, A. J. Buras, A. Poschenrieder, S. Recksiegel, C. Tarantino, S. Uhlig, and A. Weiler, *Rare and CP-Violating K and B Decays in the Littlest Higgs Model with T<sup>-</sup> Parity*, *JHEP* **01** (2007) 066, [[hep-ph/0610298](#)].
- [25] M. Blanke, A. J. Buras, and S. Recksiegel, *Quark flavour observables in the Littlest Higgs model with T-parity after LHC Run 1*, *Eur. Phys. J.* **C76** (2016), no. 4 182, [[arXiv:1507.06316](#)].
- [26] J. Reuter and M. Tonini, *Can the 125 GeV Higgs be the Little Higgs?*, *JHEP* **02** (2013) 077, [[arXiv:1212.5930](#)].
- [27] M. Tonini, *Beyond the Standard Higgs at the LHC: present constraints on Little Higgs models and future prospects*. PhD thesis, U. Hamburg, Dept. Phys., 2014.
- [28] M. E. Peskin and T. Takeuchi, *A New constraint on a strongly interacting Higgs sector*, *Phys. Rev. Lett.* **65** (1990) 964–967.
- [29] M. E. Peskin and T. Takeuchi, *Estimation of oblique electroweak corrections*, *Phys. Rev.* **D46** (1992) 381–409.
- [30] J. Hubisz, P. Meade, A. Noble, and M. Perelstein, *Electroweak precision constraints on the littlest Higgs model with T parity*, *JHEP* **01** (2006) 135, [[hep-ph/0506042](#)].
- [31] J. Berger, J. Hubisz, and M. Perelstein, *A Fermionic Top Partner: Naturalness and the LHC*, *JHEP* **07** (2012) 016, [[arXiv:1205.0013](#)].
- [32] J. Alwall, M. Herquet, F. Maltoni, O. Mattelaer, and T. Stelzer, *MadGraph 5 : Going Beyond*, *JHEP* **06** (2011) 128, [[arXiv:1106.0522](#)].
- [33] W. Kilian, T. Ohl, and J. Reuter, *WHIZARD: Simulating Multi-Particle Processes at LHC and ILC*, *Eur. Phys. J.* **C71** (2011) 1742, [[arXiv:0708.4233](#)].
- [34] M. Moretti, T. Ohl, and J. Reuter, *O’Mega: An Optimizing matrix element generator*, [[hep-ph/0102195](#)].
- [35] B. Chokoufe Nejad, T. Ohl, and J. Reuter, *Simple, parallel virtual machines for extreme computations*, *Comput. Phys. Commun.* **196** (2015) 58–69, [[arXiv:1411.3834](#)].
- [36] W. Kilian, J. Reuter, S. Schmidt, and D. Wiesler, *An Analytic Initial-State Parton Shower*, *JHEP* **04** (2012) 013, [[arXiv:1112.1039](#)].
- [37] W. Kilian, J. Reuter, and T. Robens, *NLO Event Generation for Chargino Production at the ILC*, *Eur. Phys. J.* **C48** (2006) 389–400, [[hep-ph/0607127](#)].
- [38] T. Robens, J. Kalinowski, K. Rolbiecki, W. Kilian, and J. Reuter, *(N)LO Simulation of Chargino Production and Decay*, *Acta Phys. Polon.* **B39** (2008) 1705–1714, [[arXiv:0803.4161](#)].

- [39] T. Binoth, N. Greiner, A. Guffanti, J. Reuter, J. P. Guillet, and T. Reiter, *Next-to-leading order QCD corrections to  $pp \rightarrow b$  anti- $b$   $b$  anti- $b$  +  $X$  at the LHC: the quark induced case*, *Phys. Lett.* **B685** (2010) 293–296, [[arXiv:0910.4379](#)].
- [40] N. Greiner, A. Guffanti, T. Reiter, and J. Reuter, *NLO QCD corrections to the production of two bottom-antibottom pairs at the LHC*, *Phys. Rev. Lett.* **107** (2011) 102002, [[arXiv:1105.3624](#)].
- [41] B. Chokouf  Nejad, W. Kilian, J. M. Lindert, S. Pozzorini, J. Reuter, and C. Weiss, *NLO QCD predictions for off-shell  $t\bar{t}$  and  $t\bar{t}H$  production and decay at a linear collider*, *JHEP* **12** (2016) 075, [[arXiv:1609.03390](#)].
- [42] F. Bach, B. C. Nejad, A. Hoang, W. Kilian, J. Reuter, M. Stahlhofen, T. Teubner, and C. Weiss, *Fully-differential Top-Pair Production at a Lepton Collider: From Threshold to Continuum*, [arXiv:1712.02220](#).
- [43] M. Drees, H. Dreiner, D. Schmeier, J. Tattersall, and J. S. Kim, *CheckMATE: Confronting your Favourite New Physics Model with LHC Data*, *Comput. Phys. Commun.* **187** (2015) 227–265, [[arXiv:1312.2591](#)].
- [44] J. S. Kim, D. Schmeier, J. Tattersall, and K. Rolbiecki, *A framework to create customised LHC analyses within CheckMATE*, *Comput. Phys. Commun.* **196** (2015) 535–562, [[arXiv:1503.01123](#)].
- [45] D. Dercks, N. Desai, J. S. Kim, K. Rolbiecki, J. Tattersall, and T. Weber, *CheckMATE 2: From the model to the limit*, [arXiv:1611.09856](#).
- [46] N. D. Christensen and C. Duhr, *FeynRules - Feynman rules made easy*, *Comput. Phys. Commun.* **180** (2009) 1614–1641, [[arXiv:0806.4194](#)].
- [47] A. Alloul, N. D. Christensen, C. Degrande, C. Duhr, and B. Fuks, *FeynRules 2.0 - A complete toolbox for tree-level phenomenology*, *Comput. Phys. Commun.* **185** (2014) 2250–2300, [[arXiv:1310.1921](#)].
- [48] F. Staub, *SARAH 4 : A tool for (not only SUSY) model builders*, *Comput. Phys. Commun.* **185** (2014) 1773–1790, [[arXiv:1309.7223](#)].
- [49] N. D. Christensen, C. Duhr, B. Fuks, J. Reuter, and C. Speckner, *Introducing an interface between WHIZARD and FeynRules*, *Eur. Phys. J.* **C72** (2012) 1990, [[arXiv:1010.3251](#)].
- [50] T. Sj strand, S. Mrenna, and P. Z. Skands, *A Brief Introduction to PYTHIA 8.1*, *Comput. Phys. Commun.* **178** (2008) 852–867, [[arXiv:0710.3820](#)].
- [51] **DELPHES 3** Collaboration, J. de Favereau, C. Delaere, P. Demin, A. Giammanco, V. Lema tre, A. Mertens, and M. Selvaggi, *DELPHES 3, A modular framework for fast simulation of a generic collider experiment*, *JHEP* **02** (2014) 057, [[arXiv:1307.6346](#)].
- [52] H. K. Dreiner, M. Kramer, and J. Tattersall, *How low can SUSY go? Matching, monojets and compressed spectra*, *EPL* **99** (2012), no. 6 61001, [[arXiv:1207.1613](#)].
- [53] **ATLAS** Collaboration, G. Aad et al., *Search for new phenomena in final states with an energetic jet and large missing transverse momentum in  $pp$  collisions at  $\sqrt{s} = 8$  TeV with the ATLAS detector*, *Eur. Phys. J.* **C75** (2015), no. 7 299, [[arXiv:1502.01518](#)]. [Erratum: *Eur. Phys. J.* C75,no.9,408(2015)].
- [54] J. Reuter and M. Tonini, *Top Partner Discovery in the  $T \rightarrow tZ$  channel at the LHC*, *JHEP* **01** (2015) 088, [[arXiv:1409.6962](#)].

- [55] **ATLAS** Collaboration, T. A. collaboration, *Search for supersymmetry with two and three leptons and missing transverse momentum in the final state at  $\sqrt{s} = 13$  TeV with the ATLAS detector*, .
- [56] **ATLAS** Collaboration, T. A. collaboration, *Search for squarks and gluinos in events with an isolated lepton, jets and missing transverse momentum at  $\sqrt{s} = 13$  TeV with the ATLAS detector*, .
- [57] **ATLAS** Collaboration, T. A. collaboration, *Search for squarks and gluinos in final states with jets and missing transverse momentum using  $36 \text{ fb}^{-1}$  of  $\sqrt{s} = 13$  TeV pp collision data with the ATLAS detector*, .
- [58] **ATLAS** Collaboration, T. A. collaboration, *Search for electroweak production of supersymmetric particles in the two and three lepton final state at  $\sqrt{s} = 13$  TeV with the ATLAS detector*, .
- [59] A. Collaboration, *Search for Supersymmetry at the high luminosity LHC with the ATLAS experiment*, Tech. Rep. ATL-PHYS-PUB-2014-010, CERN, Geneva, Jul, 2014.
- [60] K. Rolbiecki, “Custom Search for Sleptons and Charginos in 2 lepton final states at the high luminosity LHC.”  
["http://checkmate.hepforge.org/validationNotes/dilepton\\_HL.pdf"](http://checkmate.hepforge.org/validationNotes/dilepton_HL.pdf).
- [61] **ATLAS** Collaboration, G. Aad et al., *Search for new phenomena in final states with large jet multiplicities and missing transverse momentum at  $\sqrt{s}=8$  TeV proton-proton collisions using the ATLAS experiment*, *JHEP* **10** (2013) 130, [[arXiv:1308.1841](#)]. [Erratum: *JHEP*01,109(2014)].
- [62] **ATLAS** Collaboration, G. Aad et al., *Search for direct third-generation squark pair production in final states with missing transverse momentum and two b-jets in  $\sqrt{s} = 8$  TeV pp collisions with the ATLAS detector*, *JHEP* **10** (2013) 189, [[arXiv:1308.2631](#)].
- [63] **ATLAS** Collaboration, G. Aad et al., *Search for direct production of charginos and neutralinos in events with three leptons and missing transverse momentum in  $\sqrt{s} = 8\text{TeV}$  pp collisions with the ATLAS detector*, *JHEP* **04** (2014) 169, [[arXiv:1402.7029](#)].
- [64] **ATLAS** Collaboration, G. Aad et al., *Search for direct top-squark pair production in final states with two leptons in pp collisions at  $\sqrt{s} = 8\text{TeV}$  with the ATLAS detector*, *JHEP* **06** (2014) 124, [[arXiv:1403.4853](#)].
- [65] **ATLAS** Collaboration, G. Aad et al., *Search for direct top squark pair production in events with a Z boson, b-jets and missing transverse momentum in  $\sqrt{s}=8$  TeV pp collisions with the ATLAS detector*, *Eur. Phys. J.* **C74** (2014), no. 6 2883, [[arXiv:1403.5222](#)].
- [66] **ATLAS** Collaboration, G. Aad et al., *Search for supersymmetry at  $\sqrt{s}=8$  TeV in final states with jets and two same-sign leptons or three leptons with the ATLAS detector*, *JHEP* **06** (2014) 035, [[arXiv:1404.2500](#)].
- [67] **ATLAS** Collaboration, G. Aad et al., *Search for squarks and gluinos with the ATLAS detector in final states with jets and missing transverse momentum using  $\sqrt{s} = 8$  TeV proton-proton collision data*, *JHEP* **09** (2014) 176, [[arXiv:1405.7875](#)].
- [68] **ATLAS** Collaboration, G. Aad et al., *Search for top squark pair production in final states with one isolated lepton, jets, and missing transverse momentum in  $\sqrt{s} = 8$  TeV pp collisions with the ATLAS detector*, *JHEP* **11** (2014) 118, [[arXiv:1407.0583](#)].

- [69] **ATLAS** Collaboration, G. Aad et al., *Search for pair-produced third-generation squarks decaying via charm quarks or in compressed supersymmetric scenarios in pp collisions at  $\sqrt{s} = 8$  TeV with the ATLAS detector*, *Phys. Rev.* **D90** (2014), no. 5 052008, [[arXiv:1407.0608](#)].
- [70] **ATLAS** Collaboration, G. Aad et al., *Search for new phenomena in events with a photon and missing transverse momentum in pp collisions at  $\sqrt{s} = 8$  TeV with the ATLAS detector*, *Phys. Rev.* **D91** (2015), no. 1 012008, [[arXiv:1411.1559](#)]. [Erratum: *Phys. Rev.* **D92**,no.5,059903(2015)].
- [71] **ATLAS** Collaboration, G. Aad et al., *Search for direct pair production of a chargino and a neutralino decaying to the 125 GeV Higgs boson in  $\sqrt{s} = 8$  TeV pp collisions with the ATLAS detector*, *Eur. Phys. J.* **C75** (2015), no. 5 208, [[arXiv:1501.07110](#)].
- [72] **ATLAS** Collaboration, G. Aad et al., *Search for supersymmetry in events containing a same-flavour opposite-sign dilepton pair, jets, and large missing transverse momentum in  $\sqrt{s} = 8$  TeV pp collisions with the ATLAS detector*, *Eur. Phys. J.* **C75** (2015), no. 7 318, [[arXiv:1503.03290](#)]. [Erratum: *Eur. Phys. J.* **C75**,no.10,463(2015)].
- [73] **ATLAS** Collaboration, G. Aad et al., *ATLAS Run 1 searches for direct pair production of third-generation squarks at the Large Hadron Collider*, *Eur. Phys. J.* **C75** (2015), no. 10 510, [[arXiv:1506.08616](#)]. [Erratum: *Eur. Phys. J.* **C76**,no.3,153(2016)].
- [74] **ATLAS** Collaboration, A. Collaboration, *Search for supersymmetry at  $\sqrt{s} = 8$  TeV in final states with jets, missing transverse momentum and one isolated lepton*, .
- [75] **ATLAS** Collaboration, A. Collaboration, *Search for direct production of the top squark in the all-hadronic  $t\bar{t} + e\text{miss}$  final state in 21 fb<sup>-1</sup> of p-p collisions at  $\sqrt{s} = 8$  TeV with the ATLAS detector*, .
- [76] **ATLAS** Collaboration, T. A. collaboration, *Search for direct-slepton and direct-chargino production in final states with two opposite-sign leptons, missing transverse momentum and no jets in 20/fb of pp collisions at  $\sqrt{s} = 8$  TeV with the ATLAS detector*, .
- [77] **ATLAS** Collaboration, T. A. collaboration, *Search for strong production of supersymmetric particles in final states with missing transverse momentum and at least three b-jets using 20.1 fb<sup>-1</sup> of pp collisions at  $\sqrt{s} = 8$  TeV with the ATLAS Detector*, .
- [78] **ATLAS** Collaboration, T. A. collaboration, *Search for strongly produced supersymmetric particles in decays with two leptons at  $\sqrt{s} = 8$  TeV*, .
- [79] **ATLAS** Collaboration, T. A. collaboration, *Search for an Invisibly Decaying Higgs Boson Produced via Vector Boson Fusion in pp Collisions at  $\sqrt{s} = 8$  TeV using the ATLAS Detector at the LHC*, .
- [80] **ATLAS** Collaboration, A. Collaboration, *Search for New Phenomena in Monojet plus Missing Transverse Momentum Final States using 10fb<sup>-1</sup> of pp Collisions at  $\sqrt{s} = 8$  TeV with the ATLAS detector at the LHC*, .
- [81] **ATLAS** Collaboration, A. Collaboration, *Search for direct production of charginos and neutralinos in events with three leptons and missing transverse momentum in 21 fb<sup>-1</sup> of pp collisions at  $\sqrt{s} = 8$  TeV with the ATLAS detector*, .
- [82] **ATLAS** Collaboration, A. Collaboration, *Search for direct top squark pair production in final states with one isolated lepton, jets, and missing transverse momentum in  $\sqrt{s} = 8$  TeV pp collisions using 21 fb<sup>-1</sup> of ATLAS data*, .



- [83] **ATLAS** Collaboration, T. A. collaboration, *Search for squarks and gluinos with the ATLAS detector in final states with jets and missing transverse momentum and  $20.3 \text{ fb}^{-1}$  of  $\sqrt{s} = 8 \text{ TeV}$  proton-proton collision data*, .
- [84] **CMS** Collaboration, S. Chatrchyan et al., *Search for supersymmetry in hadronic final states with missing transverse energy using the variables  $\alpha_T$  and b-quark multiplicity in pp collisions at  $\sqrt{s} = 8 \text{ TeV}$* , *Eur. Phys. J.* **C73** (2013), no. 9 2568, [[arXiv:1303.2985](#)].
- [85] **CMS** Collaboration, V. Khachatryan et al., *Search for dark matter, extra dimensions, and unparticles in monojet events in proton-proton collisions at  $\sqrt{s} = 8 \text{ TeV}$* , *Eur. Phys. J.* **C75** (2015), no. 5 235, [[arXiv:1408.3583](#)].
- [86] **CMS** Collaboration, V. Khachatryan et al., *Search for Physics Beyond the Standard Model in Events with Two Leptons, Jets, and Missing Transverse Momentum in pp Collisions at  $\sqrt{s} = 8 \text{ TeV}$* , *JHEP* **04** (2015) 124, [[arXiv:1502.06031](#)].
- [87] **CMS** Collaboration, V. Khachatryan et al., *Search for the production of dark matter in association with top-quark pairs in the single-lepton final state in proton-proton collisions at  $\sqrt{s} = 8 \text{ TeV}$* , *JHEP* **06** (2015) 121, [[arXiv:1504.03198](#)].
- [88] **CMS** Collaboration, C. Collaboration, *Search for supersymmetry in pp collisions at  $\sqrt{s} = 8 \text{ TeV}$  in events with two opposite sign leptons, large number of jets, b-tagged jets, and large missing transverse energy*, .
- [89] **CMS** Collaboration, V. Khachatryan et al., *Search for heavy Majorana neutrinos in  $ee + jets$  and  $e\mu + jets$  events in proton-proton collisions at  $\sqrt{s} = 8 \text{ TeV}$* , *JHEP* **04** (2016) 169, [[arXiv:1603.02248](#)].
- [90] **ATLAS** Collaboration, G. Aad et al., *Search for supersymmetry at  $\sqrt{s} = 13 \text{ TeV}$  in final states with jets and two same-sign leptons or three leptons with the ATLAS detector*, *Eur. Phys. J.* **C76** (2016), no. 5 259, [[arXiv:1602.09058](#)].
- [91] **ATLAS** Collaboration, M. Aaboud et al., *Search for new phenomena in events with a photon and missing transverse momentum in pp collisions at  $\sqrt{s} = 13 \text{ TeV}$  with the ATLAS detector*, *JHEP* **06** (2016) 059, [[arXiv:1604.01306](#)].
- [92] **ATLAS** Collaboration, M. Aaboud et al., *Search for new phenomena in final states with an energetic jet and large missing transverse momentum in pp collisions at  $\sqrt{s} = 13 \text{ TeV}$  using the ATLAS detector*, *Phys. Rev.* **D94** (2016), no. 3 032005, [[arXiv:1604.07773](#)].
- [93] **ATLAS** Collaboration, M. Aaboud et al., *Search for squarks and gluinos in final states with jets and missing transverse momentum at  $\sqrt{s} = 13 \text{ TeV}$  with the ATLAS detector*, *Eur. Phys. J.* **C76** (2016), no. 7 392, [[arXiv:1605.03814](#)].
- [94] **ATLAS** Collaboration, G. Aad et al., *Search for gluinos in events with an isolated lepton, jets and missing transverse momentum at  $\sqrt{s} = 13 \text{ TeV}$  with the ATLAS detector*, *Eur. Phys. J.* **C76** (2016), no. 10 565, [[arXiv:1605.04285](#)].
- [95] **ATLAS** Collaboration, G. Aad et al., *Search for pair production of gluinos decaying via stop and sbottom in events with b-jets and large missing transverse momentum in pp collisions at  $\sqrt{s} = 13 \text{ TeV}$  with the ATLAS detector*, *Phys. Rev.* **D94** (2016), no. 3 032003, [[arXiv:1605.09318](#)].
- [96] **ATLAS** Collaboration, M. Aaboud et al., *Search for top squarks in final states with one*

*isolated lepton, jets, and missing transverse momentum in  $\sqrt{s} = 13$  TeV pp collisions with the ATLAS detector*, *Phys. Rev.* **D94** (2016), no. 5 052009, [[arXiv:1606.03903](#)].

- [97] **ATLAS** Collaboration, M. Aaboud et al., *Measurement of the  $t\bar{t}Z$  and  $t\bar{t}W$  production cross sections in multilepton final states using  $3.2\text{ fb}^{-1}$  of pp collisions at  $\sqrt{s} = 13$  TeV with the ATLAS detector*, *Eur. Phys. J.* **C77** (2017), no. 1 40, [[arXiv:1609.01599](#)].
- [98] T. A. collaboration, *A search for Supersymmetry in events containing a leptonically decaying Z boson, jets and missing transverse momentum in  $\sqrt{s} = 13$  TeV pp collisions with the ATLAS detector*, .
- [99] T. A. collaboration, *Search for production of vector-like top quark pairs and of four top quarks in the lepton-plus-jets final state in pp collisions at  $\sqrt{s} = 13$  TeV with the ATLAS detector*, .
- [100] **ATLAS** Collaboration, T. A. collaboration, *Search for top squarks in final states with one isolated lepton, jets, and missing transverse momentum in  $\sqrt{s} = 13$  TeV pp collisions with the ATLAS detector*, .
- [101] **ATLAS** Collaboration, T. A. collaboration, *Search for direct top squark pair production and dark matter production in final states with two leptons in  $\sqrt{s} = 13$  TeV pp collisions using  $13.3\text{ fb}^{-1}$  of ATLAS data*, .
- [102] **ATLAS** Collaboration, T. A. collaboration, *Further searches for squarks and gluinos in final states with jets and missing transverse momentum at  $\sqrt{s} = 13$  TeV with the ATLAS detector*, .
- [103] **ATLAS** Collaboration, T. A. collaboration, *Search for an invisibly decaying Higgs boson or dark matter candidates produced in association with a Z boson in pp collisions at  $\sqrt{s} = 13$  TeV with the ATLAS detector*, .
- [104] **CMS** Collaboration, C. Collaboration, *Search for new physics in final states with two opposite-sign same-flavor leptons, jets and missing transverse momentum in pp collisions at  $\sqrt{s} = 13$  TeV*, .
- [105] A. Collaboration, *Prospects for benchmark Supersymmetry searches at the high luminosity LHC with the ATLAS Detector*, Tech. Rep. ATL-PHYS-PUB-2013-011, CERN, Geneva, Sep, 2013.
- [106] J. S. Kim, O. Lebedev, and D. Schmeier, *Higgsophilic gauge bosons and monojets at the LHC*, *JHEP* **11** (2015) 128, [[arXiv:1507.08673](#)].